NASA Technical Memorandum 103932

Propagation Velocity and Space-Time Correlation of Perturbations in Turbulent Channel Flow

John Kim and Fazle Hussain

May 1992

National Aeronautics and Space Administration

NASA Technical Memorandum 103932

Propagation Velocity and Space-Time Correlation of Perturbations in Turbulent Channel Flow

John Kim, Ames Research Center, Moffett Field, California
Fazle Hussain, University of Houston, Houston, Texas

May 1992

National Aeronautics and
Space Administration

Ames Research Center
Moffett Field, California 94035-1000

Propagation Velocity and Space-Time Correlation of Perturbations in Turbulent Channel Flow

By John Kim† & Fazle Hussain‡

A database obtained from direct numerical simulation of a turbulent channel flow is analyzed to extract the propagation velocity V of velocity, vorticity and pressure fluctuations from their space-time correlations. A surprising result is that V is approximately the same as the local mean velocity for most of the channel, except for the near-wall region. For $y^+ \leq 15$, V is virtually constant, implying that perturbations of all flow variables propagate like waves near the wall. In this region V is 55% of the centerline velocity U_c for velocity and vorticity perturbations and 75% of U_c for pressure perturbations. Scale-dependence of V is also examined by analyzing the bandpass-filtered flow fields. This paper contains comprehensive documentation the propagation velocities and space-time correlation data, which should prove useful in the evaluation of Taylor's hypothesis. An attempt has been made to explain some of the data in terms of our current understanding of organized structures, although not all of the data can be explained this way.

1. Introduction

The propagation velocity of a perturbation in turbulent shear flow is of fundamental interest irrespective of whether turbulence is viewed as a stochastic flow field, as an assemblage of coherent structures, or as a superposition of traveling waves. From any of these viewpoints, the various flow properties and their different scales are not expected to propagate at the speed of the mean flow, nor are they always expected to propagate at identical speeds.

Recognizing what now appears to be an well-accepted notion that organized events or "coherent structures" play a dominant role in transport phenomena in turbulent flows, it is tempting to interpret V in terms of the dynamics of advecting coherent structures. [A variety of coherent structures have been proposed by various authors for turbulent boundary layers (for example, Kline et al., 1967; Willmarth and Tu, 1967; Offen and Kline, 1975; Perry and Chong, 1982; Wallace, 1985; Acarlar and Smith, 1987; Utami and Uno, 1987). For a recent survey, see Robinson (1991).]Such attempts, unfortunately, have to be relegated for now to a conceptual exercise, as the measurement required for interpretation of V in terms of coherent structures is prohibitive. On an instantaneous basis, V varies from one structure to the next; even for a given structure, V can vary considerably during its advection; different parts of a 3D structure can advect with different V; there is a variation in V across a shear flow; a flow can have a variety of coherent structures even

† NASA Ames Research Center, Moffett Field, CA 94035
‡ University of Houston, Houston, TX 77204

at a fixed station, and coherent structures can vary from one region to another in the same flow (see, for example, Hussain, 1986). Thus statistical measures of V are not only unavoidable, but also preferable as knowledge of instantaneous V during the trajectory of a structure will serve no useful purpose. Because of the statistical nature of the data, it is very difficult to interpret them in terms of instantaneous structure dynamics.

In turbulence, disturbances can be considered as superpositions of traveling waves. Their propagation may depend strongly on wavenumbers, and waves can grow and decay. In this case, several propagation velocities such as phase, group, signal and energy velocities can be defined. In general, these velocities are all different (Brillouin, 1960), especially in a frequency region where the frequency dependence (i.e. dispersion) is high and the growth or decay rate is high. Here, we are considering signal propagation velocity. The signal velocity is the velocity with which the main portion of signal amplitude travels, and it can be measured by the peak location of space-time cross correlation in an instantaneous field (for various definitions of propagation velocities deduced from velocity correlations, see Hussain and Clark, 1981). In this paper, we use propagation velocity as the signal velocity on a plane parallel to the channel wall.

Knowledge of propagation velocity has some practical applications. In aeroacoustics one needs to know the timescale of the most dominant structures that produce aerodynamic sound as well as the propagation velocity of the source. Interpretation of experimental signals or data in turbulent flows typically requires the application of Taylor's hypothesis because of problems associated with direct measurement of spatial distributions of flow variables. The hypothesis relates spatial and temporal distributions of flow variables by assuming frozen turbulence: a perturbation at (x,t) is treated as the same at $(x-Vt, t=0)$, where V is the propagation velocity of the perturbation. In spite of its widespread use (as well as equally widespread warnings against its use), there has been no rigorous test of Taylor's hypothesis itself, even though the estimated error appears to be substantial at the fine scales (Lin, 1953; Fisher and Davies, 1964; Lumley, 1965; Champagne, 1978; Piomelli et al., 1989). For example, Lin (1953) showed that Taylor's hypothesis is valid only if the turbulence intensity is low, viscous forces are negligible and the mean shear is small, thus invalidating the use of Taylor's hypothesis for most shear flows. In particular, he also showed that the error in Taylor's hypothesis is unacceptably large for the large scales in turbulent shear flow. Zaman and Hussain (1981) performed a direct evaluation of the hypothesis by educing the structures (i.e. measuring spatial details of structure properties) in an excited jet through phase-locked measurements using a reference signal without using Taylor's hypothesis, and then measuring these spatial distributions by invoking the hypothesis. They found that for the large-scale structures in a jet the error introduced by the hypothesis was surprisingly low when a single value for V equal to the advection velocity of the structure center was used everywhere across the transverse width of the shear region, except in situations where strong interactions like pairing or tearing occurred. They also showed that the typical use of either the local mean velocity or the instantaneous velocity for V produced unacceptably large errors.

Propagation velocities have been measured in a number of turbulent flows: e.g., for velocity fields in grid turbulence (Comte-Bellot and Corrsin, 1971), velocity fields in boundary

layers (Bradshaw, 1967; Bullock et al., 1978; Heidrick et al., 1977), wall pressure in turbulent boundary layers (Willmarth and Wooldridge, 1962; Dinkelacker et al., 1977; Schewe, 1983) and velocity fields in jets (Wills, 1964; Clark, 1979; Goldschmidt et al., 1981). These studies do not necessarily produce consistent results as they suffer from a number of constraints. For example, correlation measurements with a probe separation in the streamwise direction are affected by probe interference (except, of course, in non-intrusive techniques such as LDA). Such measurements have two additional constraints. They provide integral measures of propagation velocities over all scales, but the values have been found to vary significantly depending on the probe separations and time delays employed due to scale-dependence of the propagation velocity. Scale-dependent propagation velocity has been measured by Wills (1964) and Hussain and Clark (1981) by the complete Fourier transformation of space-time correlations of velocity perturbations. Direct measurement of scale-dependent propagation velocity has been attempted by narrow-band filtered data. This approach unfortunately suffers from the additional limitation that length scale discrimination is not satisfactory. For example, it is not possible to distinguish a large scale eddy moving rapidly from a smaller scale eddy moving slowly. When time delay is used along with a large spatial separation, the measurements are also biased towards the largest scales as they have longer lifetimes and dominate the correlation while the small scales decay faster because of higher dissipation.

There has been considerable confusion regarding the propagation velocity of pressure, V_p. To our knowledge, this has not been measured within a flow. Furthermore, most of surface-pressure measurements appear to be contaminated by sensor resolution (Willmarth and Wooldridge, 1962; Schewe, 1983). The propagation of pressure perturbations also has some ambiguity because pressure at a point is not truly a local property but, being the solution of the Poisson equation, is also affected by turbulent motions away from that point, i.e., everywhere within a flow domain. As such, propagation of pressure in a turbulent flow is hard to interpret. Also, one can view the instantaneous pressure as a superposition of rapid and slow pressures, being respectively associated with linear and nonlinear source terms in the Poisson equation. It would thus be interesting to examine if the propagation velocities of these two components of pressure are significantly different. If they are, the difference needs to be explained in terms of the turbulence structure. Furthermore, since a turbulent flow field consists of a superposition of rotational and irrotational flow fluctuations, there is no *a priori* reason to expect that velocity and vorticity perturbations should travel at the same speed.

This paper provides the first detailed information on propagation of velocity, vorticity and pressure perturbations in a canonical turbulent shear flow. Experimental collection of similar data has neither been achieved nor is likely to be achieved in the foreseeable future because of intrinsic limitations of the state-of-the-art measurement technology. The database used in the present work was obtained from a direct numerical simulation of turbulent channel flow by Kim, Moin and Moser (1987). The availability of the complete three-dimensional flow field as a function of time makes the use of such a database particularly attractive for the study of the propagation of perturbations in turbulent flows, which requires complete information of space-time correlations. Detailed comparisons with

existing experimental results have established the physical realism and accuracy of the computed flow fields. Many of the results presented in this paper include new information that cannot be validated directly because of the absence of experimental data, unlike most of the statistics and turbulence structures for the corresponding velocity field. However, all the statistics presented in the present work are obtained from study of the same velocity fields whose validity has been thoroughly examined, and there is little doubt that the information presented here should be valid as well.

In this paper, u, v and w denote the velocity components in the streamwise (x), transverse (y) and spanwise (z) directions, respectively, p denotes pressure, and ω_x, ω_y and ω_z denote the vorticity components in x, y and z directions, respectively. We denote the propagation velocities for these variables by $V_u, V_v, V_w, V_p, V_{\omega_x}, V_{\omega_y}$, and V_{ω_z}.

2. Review of the Database and Determination of Propagation velocity

A direct simulation of fully developed turbulent channel flow has been performed. The numerical algorithm and other details employed to generate the database can be found in Kim et al. (1987). A spectral method using the Fourier series in the streamwise and spanwise directions and a Chebychev polynomial expansion in the normal direction was used to represent the spatial distribution. Time advancement was carried out by a low-storage third-order Runge-Kutta scheme for the nonlinear terms and by the Crank-Nicolson scheme for the viscous terms. The computation was carried out using $128 \times 129 \times 128$ spectral modes in x, y and z. The Reynolds number based on the centerline velocity and the channel half-width was about 3300, and the channel half-width in wall units is about 180. The collocation grid spacings in the streamwise and spanwise directions were $\Delta x^+ \simeq 12$ and $\Delta z^+ \simeq 4$ in wall units, where the superscript + indicates a nondimensional quantity scaled by the wall variables, e.g., $y^+ = yu_\tau/\nu$, where ν is the kinematic viscosity and $u_\tau = \sqrt{\tau_w/\rho}$ is the friction velocity. A nonuniform mesh was used in the normal direction. The first mesh point away from the wall was at $y^+ \simeq 0.05$, and the maximum spacing (at the centerline of the channel) was 4.4 wall units.

Once the velocity field reached the statistical steady state, about 70 instantaneous velocity and pressure fields (each field contains about 8×10^6 words) taken at a regular time interval ($\Delta t^+ = 3$) were stored on magnetic tapes for future analyses, from which the present results were obtained. The reader is referred to Kim et al. (1987) and Kim (1989) for further details on the various turbulence statistics obtained from this calculation.

The space-time correlations, for example,

$$R_{uu}(\Delta x, y, \Delta t) = \frac{\overline{u(x,y,t)\, u(x+\Delta x, y, t+\Delta t)}}{u_{rms}(y)\, u_{rms}(y)} \tag{1}$$

are used to determine propagation velocities. There are several ways to determine propagation velocity using the space-time correlations (see Wills, 1964 and Hussain and Clark,, 1981, for example). In the present work, we used the propagation velocity determined by

$$V_i = \frac{\Delta x_{max}}{\Delta t} \tag{2}$$

Here, Δx_{max} is the streamwise separation for which $R_{ii}(\Delta x, y, \Delta t)$ is maximum for a given Δt. V_i determined in this way will be a function of the Δt used in equation (1). $\Delta t^+ = 18$ was used for the present work unless stated otherwise. The particular choice of Δt and effect of different values of Δt are discussed in the Appendix.

3. Results and Discussion

In this section we present the main results obtained by examining the channel database. In some cases, we are unable to explain some aspects of the presented results. Nevertheless, we are presenting some of these results without further discussion as no meaningful discussion appears possible with the currently available incomplete knowledge about turbulence structures in a channel or a boundary layer. We do this for archival purposes and in the hope that some of these results might prove useful to certain readers.

3.1 Propagation Velocity of Perturbations

The propagation velocities for the velocity and pressure perturbations across the channel are shown in figure 1, and those for vorticity are shown in figure 2. The same data are shown in both global and wall coordinates. It is rather surprising that for most of the outer part of the channel, say $y > 0.1\delta$, where δ is the channel half-width, the propagation velocities are essentially identical with the local mean velocity $U(y)$, being only slightly lower than $U(y)$. This implies that the turbulence structures contributing to the average propagation velocity move away from the wall so that the propagation velocity is lower than the local average.

Near the wall, however, all propagation velocities exceed $U(y)$, becoming constant ($0.55U_c$, where U_c is the mean velocity at the centerline of the channel) for $y^+ < 10$. This constant value is about the same for all perturbations except pressure. V_p is noticeably higher, $0.75\ U_c$. Since perturbations at the wall are induced by advecting dominant structures away from the wall, propagation velocity can be significant at the wall, even though the flow velocity is zero there. The propagation velocities for the three velocity components and three vorticity components are nearly equal for most of the channel, the largest discrepancy occurring around $y^+ \sim 15$.

The propagation velocity for pressure varies the least across the channel — by less than 20% of U_c — consistent with the fact that pressure is a global variable. Kim (1989) examined the source terms in the Poisson equation for pressure in order to assess the relative importance of each term and to determine the global character of the pressure fluctuations. Of the seven source terms (one linear term containing the mean shear and six nonlinear terms), it was found that $(\partial v/\partial z)(\partial w/\partial y)$ was the largest. Note that $(\partial v/\partial z)(\partial w/\partial y)$ is large at the core of streamwise vortices, and the mean square value of $(\partial v/\partial z)(\partial w/\partial y)$ has a local peak at about $y^+ = 20$, where the centers of the streamwise vortices were located on the average (Kim et al., 1987). The pressure fluctuations were therefore strongly influenced by the presence of streamwise vortices in the buffer layer. It is then not too surprising that V_p near the wall is approximately equal to V_{ω_z} at about $y^+ = 20$, and it varies much less across the channel.

To obtain further insight into the coherence of propagating perturbations, streamwise correlations of various perturbations with a fixed time delay, $R_{uu}(x)$, $R_{vv}(x)$, $R_{ww}(x)$ and $R_{pp}(x)$, were studied as functions of streamwise separation for $y^+ \simeq 5$ ($y/\delta \simeq 0.03$),

50(0.28), 100(0.57), 180(1.0), as shown in figure 3. The corresponding correlation functions for ω_x, ω_y and ω_z are shown in figure 4 for $y^+ = 5$ and 50 only. Note that the correlations are normalized such that $R_{ii}(x = 0, t = 0)$ equals 1. Near the wall, $R_{pp}(x)$ peaks at the largest x-separation, consistent with the propagation velocity data shown in figure 1. There is a slight asymmetry in $R_{pp}(x)$, the downstream front being slightly sharper. More interesting is the fact that R_{pp}, unlike all other correlations, reaches large negative values in the near-wall region. Similar negative pressure correlation has been reported by Hodgson (1971). This would suggest that pressure is more spatially distinct and oscillatory than the other variables. The $R_{pp}(\Delta x)$ data are consistent with the dominant structure educed by Jeong (1992) near the wall: namely, tilted nearly streamwise vortices with alternating signs of vorticity (figure 5). Along the line AD in figure 5, the structure induced wall pressure is oscillating in sign in x.

Further away from the wall, there is no distinction between R_{vv}, R_{ww} and R_{pp}, while R_{uu} has a much higher peak and extends for a longer x-region than the other variables, suggesting that longitudinal velocity perturbations are the most distinct and dominant features of boundary-layer turbulence. Near the wall $R_{\omega_z\omega_z}$ has the highest peak and $R_{\omega_x\omega_x}$, the lowest. Differences among $R_{\omega_x\omega_x}, R_{\omega_y\omega_y}$ and $R_{\omega_z\omega_z}$, however, disappear away from the wall, implying that vorticity fluctuations (small-scale motions) become statistically more isotropic in the outer region (Antonia et al., 1991). The similarity between R_{uu} and $R_{\omega_z\omega_z}$ near the wall is because ω_z is essentially due to $\partial u/\partial y \simeq u/y$ in the wall region. The dominance of $R_{\omega_z\omega_z}$ near the wall disappears away from the wall. It is worth noting that ω_x has the least longitudinal scale. Although many investigators had proposed earlier an eddy structure that consisted of a pair of counter-rotating vortices that are elongated in the streamwise direction and are parallel to the wall (Blackwelder, 1978; Blackwelder and Eckelmann, 1979), Moin and Kim (1985) disputed this model based on the results obtained from their simulation. Kim and Moin (1986) contended that streamwise vortices convecting downstream without losing their coherence for long distance (over 1000 ν/u_τ) had given the false impression that the streamwise extent of these vortices was rather long. The present results support the notion that the streamwise vortices are relatively short in the streamwise direction but temporally persistent. The dominant and largest scale of R_{uu}, of course, is consistent with the streaks observed by Kline et al. (1967) and others.

3.2 Transverse Correlations of Perturbations

To examine the transverse (inhomogeneous direction) characteristics of turbulence structure in the channel, transverse correlation distributions with zero time delay, for example,

$$R_{uu}(y_r, y) = \frac{\overline{u(y_r)\, u(y)}}{u_{rms}(y_r)\, u_{rms}(y)} \tag{3}$$

where y_r is the reference transverse location, have been computed. $R_{uu}(y_r, y)$, $R_{vv}(y_r, y)$, $R_{ww}(y_r, y)$ and $R_{pp}(y_r, y)$ for y_r values corresponding to $y^+ \simeq 5$, 50, 100 and 180 are shown in figures 6(a)-(d). In addition, $R_{pp}(y, y_r)$ for $y_r = 0$ is given in figure 6(e). The corresponding $R_{\omega_x\omega_x}$, $R_{\omega_y\omega_y}$ and $R_{\omega_z\omega_z}$ correlations for $y_r = 0.03\delta$ ($y^+ \simeq 5$) and $y_r = \delta$ ($y^+ \simeq 180$) are shown in figure 7. As is clear from figures 6(a,b), the pressure field is fairly well correlated over a large width of the channel. This is consistent with the high value

of V_p near the wall, if one assumes that pressure at the wall is induced by the structures farther away from the wall. Unlike vorticity or velocity components, there is a significant correlation between pressure at the wall and pressure at the channel centerline. For instance, at $y_r = 0.03\delta$, velocity correlation drops to 0 at $y = 0.2\delta$, but the pressure correlation decreases gradually, dropping to only 0.3 at $y \simeq 0.5\delta$, then to 0.15 at the channel center ($y = \delta$). The global dependence of quantities associated with pressure has been reported by Kim (1989), who presented pressure and pressure-strain correlations in terms of a Green's function. Because of the nonlocal nature of the pressure fluctuations, the contributions to pressure-strain terms were also nonlocal, especially away from the wall region, raising serious doubt as to whether one can model them in terms of local variables as is currently done. R_{uu}, R_{vv} and $R_{\omega_y\omega_y}$ drop monotonically while R_{ww}, $R_{\omega_x\omega_x}$ and $R_{\omega_z\omega_z}$ show negative excursions in their correlations. These negative values are consistent with quasi-streamwise vortices as the dominant structure (fig. 5). The negative value of $R_{\omega_x\omega_x}$ results from the no-slip boundary condition at the wall, where a quasi-streamwise vortex induces streamwise vorticity of the opposite sign adjacent to the wall. A quasi-streamwise vortex also induces w-velocity with negative $R_{ww}(y_r, y)$ if y_r and y are located across the vortex center [fig. 8(a)]. Since the streamwise vortical structure creates "uv2" and "uv4" events on its sides, the associated streamwise velocity perturbation and its y-derivative $\partial u/\partial y \approx \omega_z$ will have oscillations in the y direction [fig. 8(b)]. These explanations are consistent with previous observations made by other investigators: Moin and Kim (1985) showed the negative excursions in $R_{ww}(y)$ are caused by horseshoe-like vortices; the internal shear-layer structures studied by Jimenez et al. (1987) and Johansson et al. (1987, 1991) produced the negative excursion in $R_{\omega_x\omega_x}(y)$ and $R_{\omega_z\omega_z}(y)$. The peak value of the negative correlations is lower toward the channel center, suggesting that structures are less clearly defined there. The correlation length increases continuously until the channel center; those of p and v are the largest, and that of w is the smallest.

3.3 Scale-Dependence of Propagation Velocity

In order to determine the scale-dependence of propagation velocities, the flow field was divided into eight equi-spaced streamwise wavenumber (k_x) ranges. This is approximately equivalent to bandpass filtering temporal signatures in an experiment. The time delay ($\Delta t^+ = 18$) turned out to be too large for large wavenumbers. The time scales associated with small-scale motions (corresponding to large wavenumbers) are small, and the maximum correlations for large wavenumbers with $\Delta t^+ = 18$ becomes too small to accurately determine the location of the peak correlations. Hence, for this particular study, $\Delta t^+ = 3$ was used instead. All the results presented in the present subsection are normalized by the propagation velocity for all scales (i.e., no bandpass filtering) using $\Delta t^+ = 3$.

Except near the wall, no noticeable k_x-dependence of the propagation velocities was found. As an example, these variations are shown in figure 9. Contrary to the expectation that larger scales have higher propagation speeds, the data show the k_x-dependence to be marginal. Near the wall, the largest scales of u and ω_z move slower while smaller scales of u and ω_z move faster, although the variation is rather small. Beyond $y^+ = 12$, there is no noticeable k_x-dependence.

The dependence of V on the spanwise scale is similarly determined by dividing the flow field into eight equi-spaced spanwise wavenumber (k_z) ranges. The k_z-dependence

Table 1

Scale Dependence of Propagation Velocity

Scales	k_x	k_z	V_{g_x}	V_{g_z}
Large in x, large in z	Small	Small	Large	Small
Large in x, small in z	Small	Large	Small	Small
Small in x, large in z	Large	Small	Large	Large
Small in x, small in z	Large	Large	Small	Large

of V is much more dramatic (fig. 10). The k_z-dependence is monotonic near the wall; there is a two-fold increase in V with an eight-fold increase in scale. Note that the scale-dependence seems to be fairly similar for all the variables except for pressure, which shows a rather strong scale dependence (at $y^+ = 12$). The k_z-dependence decreases away from the wall, being negligible for $y^+ \geq 50$ (not shown here). Note also that even though V_p is the largest near the wall, $V_p(k_z)$ shows the lowest values because it is normalized by the corresponding propagation velocity for all scales. The strong k_z-dependence near the wall is indeed intriguing, but perhaps can be explained in terms of the small-scale motion produced near the wall. Assuming that small-scale (random) turbulence produced near the wall is advected passively, the propagation velocity of the small scales is lower than that of the (large-scale) streaks, because the propagation of streaks is controlled by the structures away from the wall, which move faster (fig. 11). This view is consistent with the streak-formation mechanism proposed by Moin and Kim (1985), in which the streaks are produced by streamwise vortices convecting at a higher velocity than the local mean velocity.

The above scenario and the k_z-dependence have further implications. If we consider propagation velocity as the group velocity V_g of a perturbation wave, the value of V_g in the streamwise direction is essentially a function of k_z only; i.e., $V_{gx} = V(-a|k_z| + b) = f(k_z)$ where V is the propagation velocity of all scales, a = 0.01 and b = 1.1 (fig. 10). Here, $|k_z|$ indicates a symmetry in z. Since $V_{gx} = \partial\Omega/\partial k_x = f(k_z)$, where Ω is the frequency, $\Omega \sim k_x f(k_z)$. Now the group velocity in the spanwise direction is $V_{gz} = \partial\Omega/\partial k_z = k_x f'(k_z) = \pm a k_x$. This implies that the large-scale streaks (small k_x) do not wander significantly in the spanwise direction, but small scales do presumably due to the induced motion by the streamwise vortices (fig. 11). The k_x and k_z dependencies of propagation velocities V_{g_x} and V_{g_z} are given in Table 1. The weak dependence of V_{g_z} on k_x results from the k_z-dependence; the energy spectra in the streamwise direction, from which V_{gx} is computed, are summed over all k_z, and the spectra for small k_x are likely to be influenced more by small k_z, resulting in the weak k_x-dependence.

3.4 Space-Time Correlations

Turbulent perturbations are not passively advected but undergo evolutionary changes.

Thus a perturbation field changes its size, deforms in shape, as well as moves in the streamwise, transverse and spanwise directions. Consequently, a more complete understanding of the propagation of a perturbation can be achieved by further examining space-time correlations with streamwise and transverse separations. These provide not only some perceptions of the propagation of the perturbation field, but also their evolution in space and time. In the following, we first discuss correlation in (x,t)-space and then in the (x,y)-plane with a time delay. These figures represent a significant amount of information on turbulence structure in channel flow even though we are not necessarily able to interpret them completely now. These, included for archival purposes and for modeling efforts by others, provide vivid depictions of the perturbation fields and their propagation.

Contours of $R_{pp}(\Delta x,\Delta t)$, $R_{\omega_x\omega_x}(\Delta x,\Delta t)$ and $R_{\omega_z\omega_z}(\Delta x,\Delta t)$ at $y=0$ are shown in figure 12, and contours of $R_{uu}(\Delta x,\Delta t)$, $R_{vv}(\Delta x,\Delta t)$, $R_{ww}(\Delta x,\Delta t)$, $R_{pp}(\Delta x,\Delta t)$, $R_{\omega_x\omega_x}(\Delta x,\Delta t)$, $R_{\omega_y\omega_y}(\Delta x,\Delta t)$, and $R_{\omega_z\omega_z}(\Delta x,\Delta t)$ at $y^+=12$ are shown in figure 13. The figures show that all perturbations considered here propagate in a nondispersive manner (consistent with k_x- independence discussed earlier); i.e., the width of the constant contour levels in the spatial direction does not spread with time, and the propagation velocities do not appear to be too dependent on the time delay as indicated by the alignment of the ridges of the maximum correlations with a constant slope line. The contours also show that the correlations associated with the streamwise velocity (R_{uu}, in particular, and to some extent $R_{\omega_y\omega_y}$) have larger correlation lengths both in time and space. Contours for R_{pp} and $R_{\omega_x\omega_x}$ show shorter correlation lengths in the streamwise direction (consistent with shorter integral length scales of p and ω_x compared with that of u). Note also that R_{pp} has negative contours near the wall unlike the other correlations.

The correlations R_{uu}, R_{vv}, R_{ww}, R_{pp}, $R_{\omega_x\omega_x}$, $R_{\omega_y\omega_y}$ and $R_{\omega_z\omega_z}$ with zero time delay in the (x,y)-plane with the reference probe located at $y_r^+=12$ and $y_r^+=100$ are shown in figures 14 and 15. Note that all the correlations are normalized by their local variance [eqn. (3)], and they have their peaks at the reference location. These contours, except those for p and v, show quite well that the dominant structures are inclined at an angle to the wall. The contours for $R_{\omega_z\omega_z}$ have a strong resemblance to the shear-layer structure studied by Jimenez et al. (1987) and Johansson et al. (1987, 1991). The implication is that these shear layers are so dominant that their influence is strong even on the long-time averaged statistics such as the two-point correlations. Johansson et al. (1991) reported that the production for turbulent kinetic energy per unit volume associated with the shear layers was about three times larger than that of the rest of the flow.

Pressure is well correlated in the transverse direction; so is v, but its streamwise extent is considerably shorter. Pressure correlation extends transversely, essentially normal to the wall. The long transverse correlation of p again suggests that p is not a local flow variable but bears the footprint of flow structures in the channel core (see Kim, 1989). The pressure difference near the wall across the channel is marginal, even though a streamwise vortical structure is present: e.g., $\partial p^+/\partial y^+ = -\partial\omega_x^+/\partial z^+ + \partial\omega_z^+/\partial x^+ \approx -\partial\omega_x^+/\partial z^+ \sim 0.4/20 = 0.02 << 1$ in wall units, considering a quasi-streamwise structure located in the buffer region (Kim et al., 1987). That is, the boundary condition for pressure at the wall behaves essentially as a mirror (Kraichnan, 1956). It has also been shown by Kim (1989) that the contribution from the inhomogeneous boundary condition and homogeneous equation

for the Stokes pressure is negligibly small. The mirror boundary condition on both walls in the channel creates an infinite number of sources aligned in the transverse direction. These image sources for pressure are responsible for the surprisingly high correlation in the transverse direction, even extending from the wall to the channel centerline. In the boundary layer where there is only one wall, pressure is not likely to behave in this manner.

The correlation of u extends over a much bigger area, consistent with the long streaky structures observed in flow visualization, but the length scales for the organized vorticity fields are rather short. This is also a strong argument against basing detection and eduction schemes on the u-signal only. If coherent structures are defined in terms of the vorticity field (Hussain, 1980), then the detection and eduction of coherent structures must be based on vorticity. The u-signal alone is insensitive to the details of the organized structures characterized by coherent vorticity.

Further away from the wall (fig. 15) all the correlations decrease rapidly except for R_{uu}. Toward the center of the channel (not shown here), ω_x and ω_z correlations decrease in area and strength, while ω_y correlations continue to be dominant. This is consistent with the tips of hairpin structures being more aligned with y-axis at larger y.

Correlations at nonzero time delay, $R_{ii}(\Delta x, y_r^+ = 12, \Delta t^+ = 18)$, are shown in figure 16. The impression just described regarding propagation of velocity, pressure and vorticity is confirmed. The pressure field propagates downstream while remaining virtually aligned in the normal direction; the velocity and vorticity correlations suggest inclined flow structures, with the near-wall part trailing the part in the channel centerline. The significantly higher correlations of u, compared to those of other variables, are consistent with the persistence of near-wall streaks.

3.5 Rapid and Slow Pressure

The profile of the propagation speed as well as correlation contours for pressure are noticeably different from those for other variables. In order to obtain further understanding of this behavior, it was felt worthwhile to examine correlations and propagation velocities corresponding to the rapid (linear) and slow (nonlinear) pressure separately. Figure 17 shows the propagation velocity profiles for the rapid (p_r), slow (p_s) and total (p_t) pressure. V_{p_r} is higher than V_{p_s} near the wall while the reverse holds in the center of the channel, although the difference is rather small.

Figure 18 shows correlations in the (x, y)-plane of p_r and p_s for $\Delta t^+ = 18$. It is clear that the correlation of p_r extends in the transverse direction much more than that of p_s, while correlation of p_s shows inclined structure unlike that of p_r. Contours of rapid pressure have negative parts, but those for slow pressure do not, indicating that the negative correlation associated with the total pressure is due to the rapid pressure. The conditionally averaged pressure fluctuations associated with the near-wall shear layers (Johansson et al., 1991) had a large positive peak surrounded by negative pressure lobes. Examination of our results suggest that the positive peak is due to the slow pressure while the negative lobes are due to the rapid pressure. Although the rapid and slow pressures play distinct roles, there appears to be no striking difference between their behavior as far as propagation speeds are concerned. We also note that the location of peak correlation moves away from the wall in time, suggesting that the source of pressure (i.e., structure) moves in time away from the wall.

4. Summary and Concluding Remarks

There is a dearth of data on propagation velocity, primarily because of the enormous experimental effort involved as well as the inherent experimental constraints. The direct numerical simulation data afford the opportunity to determine propagation velocities of pressure, velocity, vorticity and velocity gradient perturbations and their space-time correlations with more accuracy than is likely in experiments.

Propagation velocities are studied by analyzing a database obtained from a well-tested numerical simulation of channel flow. Contrary to the widespread belief, for most of the channel, the propagation velocities for velocity, pressure and vorticity are approximately equal to the local mean velocity. In the wall region, the propagation velocities approach a constant value ($0.55U_c$) except that of pressure, which attains a higher constant value ($0.75U_c$). The distinctly different value for pressure, though surprising, is consistent with the fact that pressure is a nonlocal variable. Propagation of pressure perturbations is strongly influenced by the streamwise vortices in the buffer layer and thus varies little across the channel.

Scale-dependence of the propagation velocity is examined by analyzing flow fields obtained by bandpass filtering (in wave space) the original fields. It is shown that, away from the wall, the propagation velocity is independent of wavenumbers. In the wall region, there is weak dependence on the streamwise scale but a rather strong dependence on the spanwise scale. We have attempted to explain this difference in terms of the dynamics of fine-scale turbulence near the wall and (large-scale) streaks. The explanation seems to lie with the fact that the near-wall flow consists of structures with distinct spanwise scales which persist, while there is no such persistence of streamwise scales.

Dependence of the propagation speed on the time delay is also examined. The variation is the largest for pressure in the wall region. The difference between V_p and others for dependencies on Δt^+ is somewhat surprising in view of the fact that pressure is supposed to behave like a global property, being largely dominated by the outer flow. In that case, pressure near the wall should have longer time scales than velocity; thus, V_p should be relatively insensitive to Δt^+. Of course, we also know from experimental data (Emmerling, 1973) and from a comparison of u and p contours at $y^+ = 5$ (fig. 14) that pressure indeed has smaller scales than velocity in the streamwise direction, though not smaller than vorticity. Pressure correlation will thus be expected to be dependent on Δt^+. The interesting feature of the pressure correlation is that it is compact in the streamwise direction but extended in the transverse direction. This is quite a contrast with the velocity and vorticity fields, particularly u.

Many features observed from the space-time correlations presented in the present paper resemble those dominant structures obtained either from a single realization or a conditionally-averaged field. This suggests, in turn, that those structures are so dominant that they leave their imprints even in the time-averaged statistics. This is contrary to the common belief that time-averaged statistics do not contain any structural information. Proper orthogonal decomposition (Lumley, 1981; Moin and Moser, 1989) and linear stochastic estimation (Adrian and Moin, 1988) are good examples which illustrate that one can extract much information on organized structures from such time-averaged statistics if one makes judicious choice of available statistical analyses.

Hussain et al. (1987) studied the effect of the propagation velocity on the error associated with the Taylor's hypothesis in the channel flow. The local mean velocity, local instantaneous velocity and a filtered velocity were used as the propagation velocity. They found that the error was rather small for all cases except in the near-wall region. The present results indicate that the propagation velocity in the wall region deviates significantly from the mean velocity. It should be interesting to see if the use of the constant propagation velocity found in the present study will reduce the errors. One can also determine the velocity $\mathbf{V}(\mathbf{x},t)$ directly from the numerical simulation such that Taylor's hypothesis $\partial\mathbf{u}/\partial t + \mathbf{V}(\mathbf{x},t)\cdot\nabla\mathbf{u} = 0$ is satisfied. It would be interesting to examine how mean values $< \mathbf{V}(\mathbf{x},t) >$ compare with the propagation velocities reported in this paper.

We are grateful to Mr. Jinhee Jeong of University of Houston for allowing us to use some unpublished data, and for the assistance during the course of this work. Drs. Robert Moser and Michael Rogers of NASA Ames Research Center made many helpful comments on a draft of this paper.

APPENDIX : Dependence of Propagation Velocity on Time Delay

The computed (or measured) propagation velocity, determined as explained in section 2, would depend on the value of the time delay used, because the time scales associated with different scales of motions are different. For instance, time scales associated with small eddies would be much smaller than those associated with large eddies, and if a large time delay is used, only the propagation of large scale motions would be reflected. Furthermore, with a large time delay, the maximum value of the correlation function becomes too small and less peaky. This would result in a large error in determining the propagation velocity. On the other hand, if too small a time delay were used, only small-scale motions would be reflected in the propagation velocity. Also, with both Δx_{max} and Δt being small, a large error could result. This is particularly critical in analyzing the computed database, because one has to interpolate between grid points to determine Δx_{max}. In the present study we interpolate spectrally to minimize the error associated with the interpolation procedure. The interpolation error can become significant, nonetheless, if Δx_{max} is too small.

$\Delta t^+ = 18$ was chosen because this time delay not only gave reasonable peak values for all quantities considered (varying from 0.4 to 0.8 depending on the perturbation and y-location) but also gave Δx_{max} larger than 10 grid spacings in the streamwise direction, corresponding to a maximum possible interpolation error less than 10%. The actual interpolation error, however, is negligible because of the spectral interpolation used.

To examine the dependency of the computed propagation velocity on the time delay, three different time delays, $\Delta t^+ = 3, 18$ and 27, were tried. Except for very close to the wall ($y^+ < 12$), no variation of the propagation velocities was found within this range of Δt^+. Close to the wall, however, the dependence on Δt^+ was striking, but not unlike that found by Willmarth and Wooldridge (1962) and Corcos (1964). For example, at $y^+ = 5$, between $\Delta t^+ = 3$ and 27, V_u changed by about 5% while V_p changed by about 18%. For the computation of the overall propagation velocities in this paper, we have used $\Delta t^+ = 18$. However, for the bandpass-filtered propagation velocities (see section 3.3), $\Delta t^+ = 18$ was found to be too large for high wavenumber ranges; for these we used $\Delta t^+ = 3$ for all wave numbers.

REFERENCES

Acarlar, M. S. and Smith, C. R. A study of hairpin vortices in a laminar boundary layer. Part 1. Hairpin vortices generated by a hemisphere protuberance. *J. Fluid Mech.*, **175**, p1, 1987.

Adrian, R. J. and Moin, P. Stochastic estimation of organized turbulent structure: Homogeneous shear flow. *J. Fluid Mech.*, **190**, p531, 1988.

Antonia, R. A., Kim, J. Kim and Browne, L. W. B. Some characteristics of small scale turbulence in a turbulent duct flow. *J. Fluid Mech.*, **233**, p369, 1991.

Blackwelder, R. F. The bursting process in turbulent boundary layers. In *Coherent Structure of Turbulent Boundary Layers*, C. R. Smith and D. E. Abbott (Eds.), AFOSR/Lehigh University Workshop, Dept. Mech. Engng and Mech., Bethlehem, PA, 1978.

Blackwelder, R. F. and Eckelmann, H. Streamwise vortices associated with the bursting phenomenon. *J. Fluid Mech.*, **94**, p577, 1979

Bradshaw, P. 'Inactive' motion and pressure fluctuation in turbulent boundary layer. *J. Fluid Mech.*, **27**, p209, 1967.

Brillouin, L. Wave propagation and group velocity. Academic Press, 1960.

Bullock, K. J., Cooper, R. E. an Abernathy. F. H. Structural similarity in radial correlations and spectra of longitudinal velocity fluctuation in pipe flow. *J. Fluid Mech.*, **88**, p585, 1978.

Champagne, F. H. The fine-scale structure of the turbulent velocity field. *J. Fluid Mech.*, **86**, p67, 1978.

Clark, A. R. Experimental study of the coherent motions in an axisymmetric mixing layer. Ph. D. Dissertation, Univ. of Houston, 1979.

Comte-Bellot, G. and Corrsin, S. Simple Eulerian correlation of full- and narrow-band velocity signals in grid-generated, 'isotropic' turbulence. *J. Fluid Mech.*, **48**, p273, 1971

Corcos, G. M. The structure of the turbulent pressure field in boundary-layer flows. *J. Fluid Mech.*, **18**, p353, 1964.

Dinkelacker, A., Hessel, M., Meier, G. E. A. and Schewe, G. Investigation of pressure fluctuations beneath a turbulent boundary layer by means of an optical method. *Phys. Fluids*, **20**, No. 10, S216, 1977

Emmerling, R. The instantaneous structure of the wall pressure under a turbulent boundary layer flow. *Max-Planck-Institut für Strömungsforschung Rep. No. 9/1973*, 1973.

Fisher, M. J. and Davies, P. O. A. L. Correlation measurements in a non-frozen pattern of turbulence. *J. Fluid Mech.*, **18**, p97, 1964.

Goldschmidt, V. W., Young, H. F. and Ott, E. S. Turbulent convective velocities (broadband and wavenumber dependent) in a plane jet. *J. Fluid Mech.*, **105**, p327, 1981.

Heidrick, T. R., Banerjee, S. and Azad, R. S. Experiments on the structure of turbulence in fully developed pipe flow: interpretation of the measurements by a wave model. *J. Fluid Mech.*, **81**, p137, 1977.

Hodgson, T. H. On the dipole radiation from a rigid and plane surface. Proc. Purdue Noise Control Conf., 1971.

Hussain, A. K. M. F. Lecture notes in physics, vol. 136, p. 252. Springer, 1980.

Hussain, A. K. M. F. Coherent structures and turbulence. *J. Fluid Mech.*, **173**, p303, 1986.

Hussain, A. K. M. F. and Clark, A. R. Measurements of wavenumber- celerity spectrum in plane and axisymmetric jets. AIAA, **19** No. 1, p51, 1981.

Hussain, A. K. M. F., Jeong, J. and Kim, J. Structure of turbulent shear flows. In *Proc. of the 1987 Summer Program, CTR-S87*, Center for Turbulence Research, NASA Ames-Stanford, 1987.

Jeong, J. Ph. D. Dissertation, Univ. of Houston, in preparation, 1992.

Jimenez, J., Moin, P. Moser, R. D. and Keefe, L. R. Ejection mechanisms in the sublayer of a turbulent channel. In *Proc. of the 1987 Summer Program, CTR-S87*, Center for Turbulence Research, NASA Ames-Stanford, 1987.

Johansson, A. V., Alfredsson, P. H. and Kim, J. Shear-layer structures in near-wall turbulence. In *Proc. of the 1987 Summer Program, CTR-S87*, Center for Turbulence Research, NASA Ames-Stanford, 1987.

Johansson, A. V., Alfredsson, P. H. and Kim, J. Evolution and dynamics of shear-layer structures in near-wall turbulence. *J. Fluid Mech.*, **224**, p579, 1991.

Kim, J. On the structure of pressure fluctuations in simulated turbulent channel flow. *J. Fluid Mech.*, **205**, p421, 1989.

Kim, J. and Moin, P. Flow structures responsible for the bursting process. Bull. American Physical Society, **31**, no 10, 1986.

Kim, J., Moin, P. and Moser, R. D. Turbulence statistics in fully developed channel flow at low Reynolds number. *J. Fluid Mech.*, **177**, p133, 1987.

Kline, S. J., Reynolds, W. C., Schraub, F. A. and Rundstadler, P. W The structure of turbulent boundary layers. *J. Fluid Mech.*, **30**, p741, 1967.

Kraichnan, R. H. Pressure fluctuations in turbulent flow over a flat plate. J. Acoust. Soc. **28**, p378, 1956.

Lin, C. C. On Taylor's hypothesis and the acceleration terms in the Navier-Stokes equation. *Quart. Appl. Math*, **10**, p295, 1953.

Lumley, J. L. Interpretation of time spectra measure in high-intensity shear flows. *Phys. Fluids*, **8**, No. 6, p1056, 1965.

Lumley, J. L. Coherent structures in turbulence. In *Transition and Turbulence* (R. E. Meyer, ed.), Academic Press, 1981.

Moin, P. and Kim, J. The structure of the vorticity field in turbulent channel flow. Part 1, Analysis of instantaneous fields and statistical correlations. *J. Fluid Mech.*, **155**, p441, 1985.

Moin, P. and Moser, R. D. Characteristic eddy decomposition of turbulence in a channel. *J. Fluid Mech.*, **200**, p471, 1989.

Offen, G. R. and Kline, S. J. A proposed model of the bursting process in turbulent boundary layers. *J. Fluid Mech.*, **70**, p209, 1975.

Perry, A. E. and Chong, M. S. On the mechanism of wall turbulence. *J. Fluid Mech.*, **119**, p173, 1982.

Piomelli, U., Balint, J. L. and Wallace, J. M. On the validity of Taylor's hypothesis for wall-bounded turbulent flows. *Phys. Fluids A*, **1**, p609, 1989.

Robinson, S. K. Coherent motions in the turbulent boundary layer, *Annu. Rev. Fluid Mech*, **16**, p99, 1991.

Schewe, G. On the structure and resolution of wall-pressure fluctuations associated with turbulent boundary layer flow. *J. Fluid Mech.*, **134**, p311, 1983.

Utami, T. and Uno, T. Experimental study on the coherent structure of turbulent open-channel flow using visualization and picture processing. *J. Fluid Mech.*, **174**, p399, 1987.

Wallace, J. M. The vortical structure of bounded turbulent shear flow. In Lecture Notes in Physics 235, Springer-Verlag, 1985.

Willmarth, W. W. and Tu, B. J. Structure of turbulence in the boundary layer near the wall. *Phys. Fluids*, **10**, S134, 1967.

Willmarth, W. W. and Wooldridge, C. E. Measurements of the fluctuating pressure at the wall beneath a thick turbulent boundary layer. *J. Fluid Mech.*, **14**, p187, 1962.

Wills, J. A. B. On convection velocities in turbulent shear flows. *J. Fluid Mech.*, **20**, p417, 1964.

Zaman, K. B. M. Q. and Hussain, A. K. M. F. Taylor hypothesis and large- scale coherent structures. *J. Fluid Mech.*, **112**, p379, 1981.

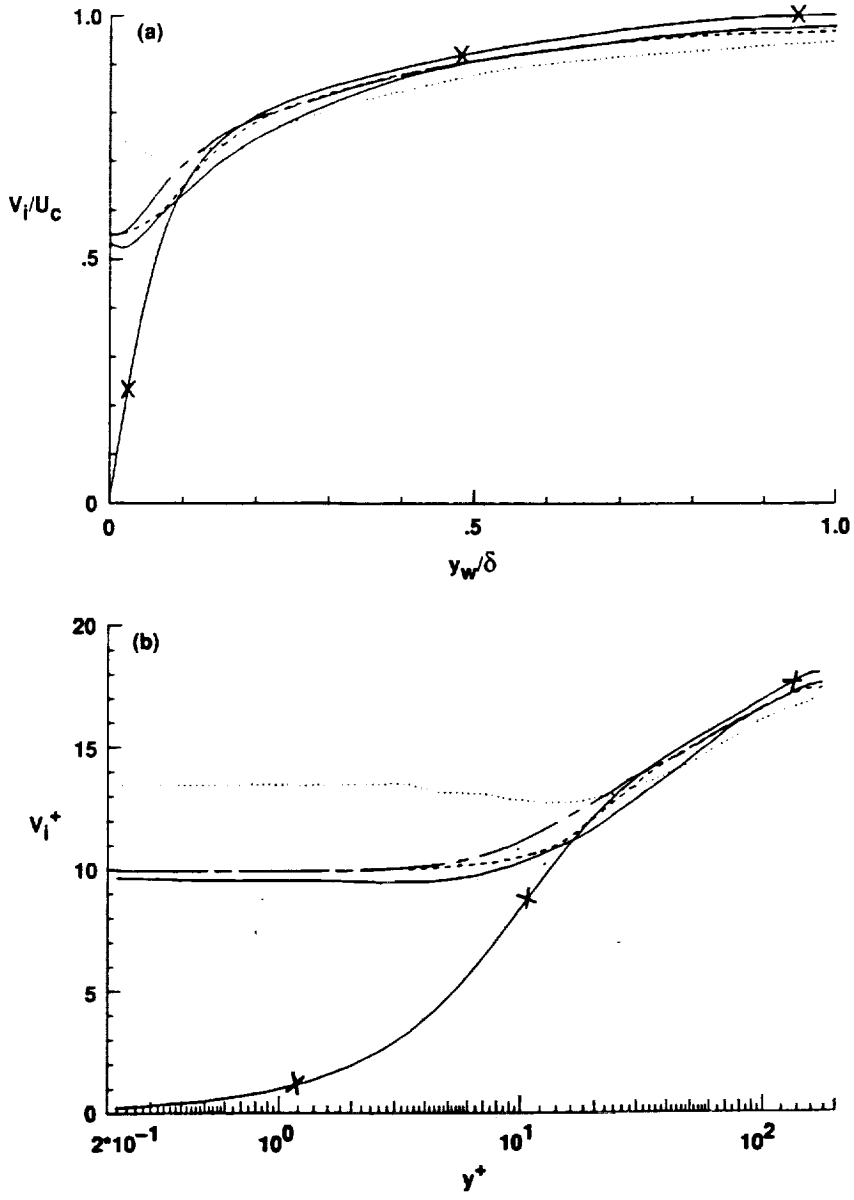

Figure 1. Propagation velocities for the velocity and pressure perturbations across the channel (a) in global coordinate and (b) in wall coordinate: —×— , mean; ——— , V_u; - - - - , V_v; — — — , V_w; ····· , V_p.

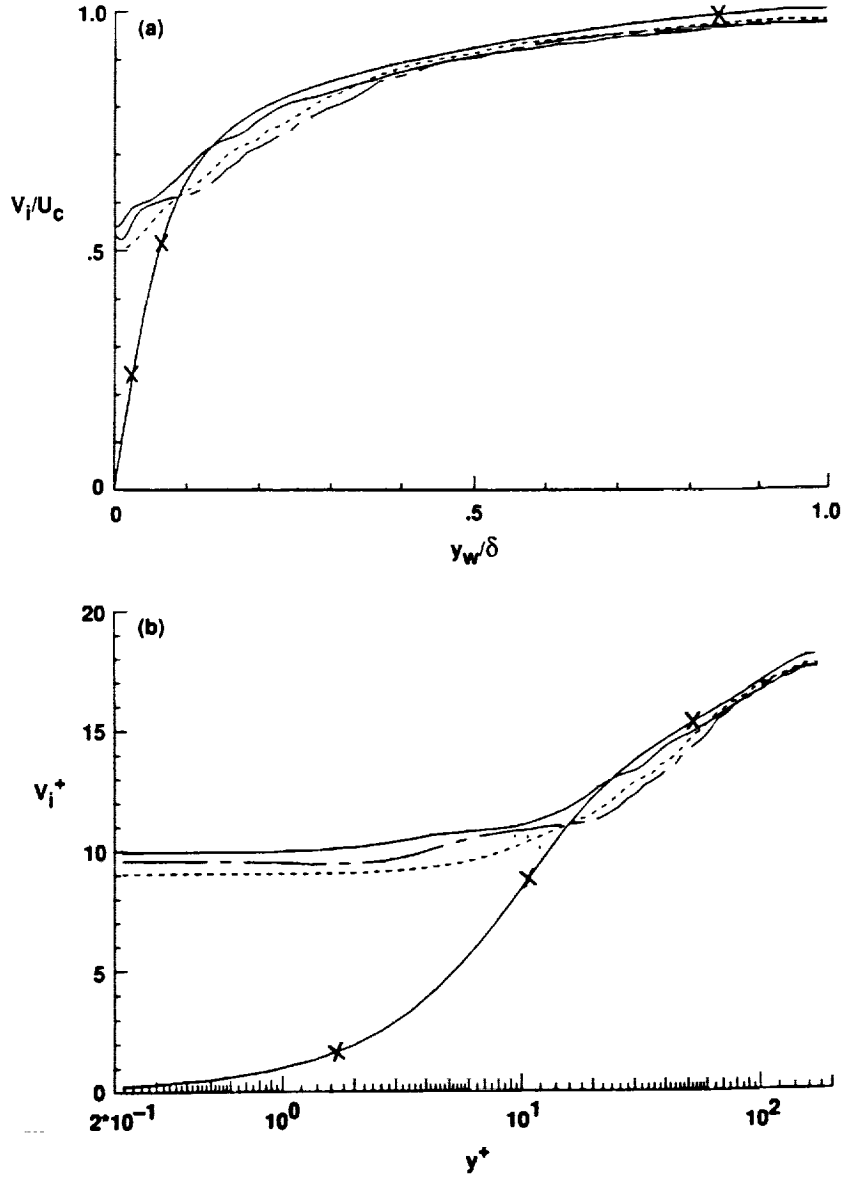

Figure 2. Propagation velocities for the vorticity perturbations across the channel (a) in global coordinate and (b) in wall coordinate: —×— , mean; ——— , ω_x; - - - - , ω_y; — — — , ω_z.

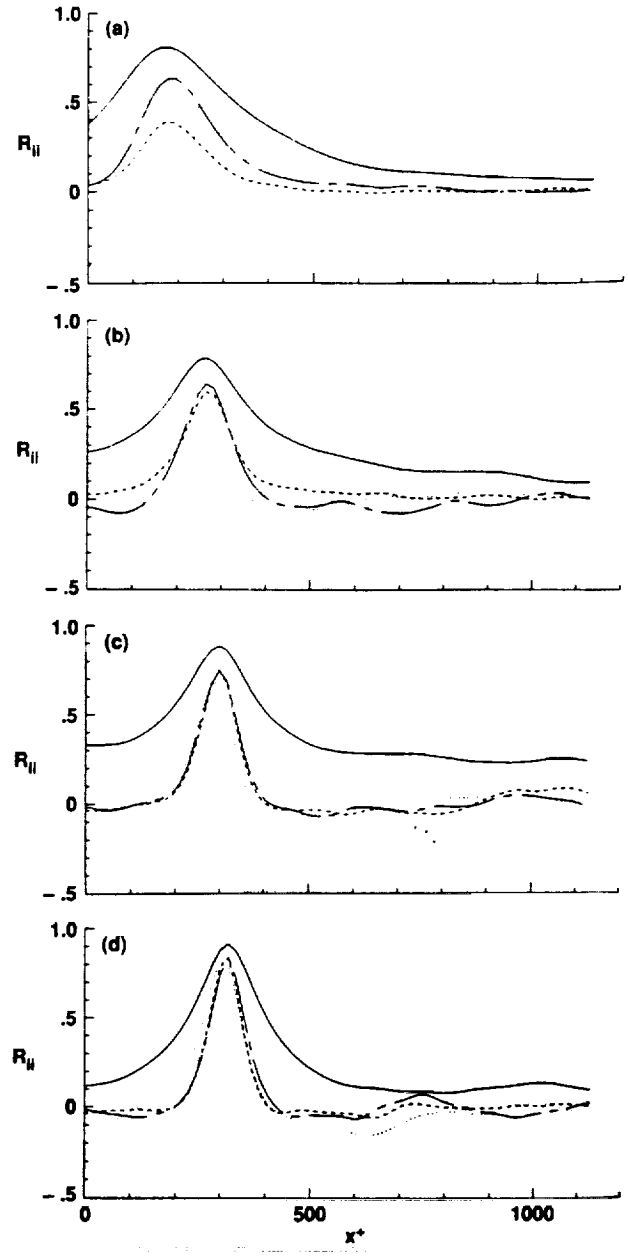

Figure 3. Streamwise correlations of perturbations with a fixed time delay (a) at $y^+ \simeq 5$, (b) at $y^+ \simeq 50$, (c) at $y^+ \simeq 100$, (d) at $y^+ \simeq 180$: ——— , R_{uu}; ---- , R_{vv}; —-— , R_{ww}; ..... , R_{pp}.

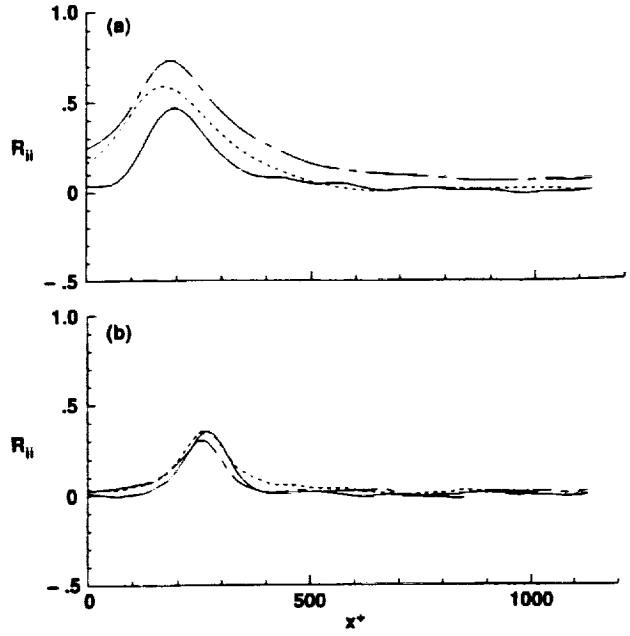

Figure 4. Streamwise correlations of perturbations with a fixed time delay (a) at $y^+ \simeq 5$, (b) at $y^+ \simeq 50$: ——— , $R_{\omega_x\omega_x}$; ---- , $R_{\omega_y\omega_y}$; —·— , $R_{\omega_z\omega_z}$.

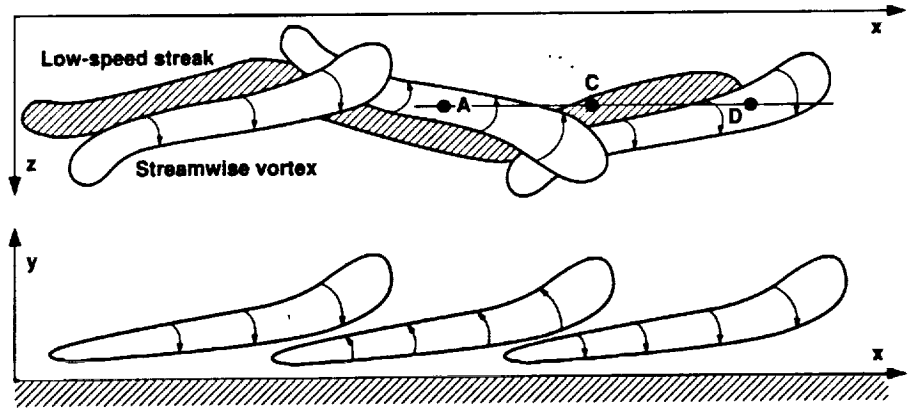

Figure 5. A conceptual model of near-wall structure.

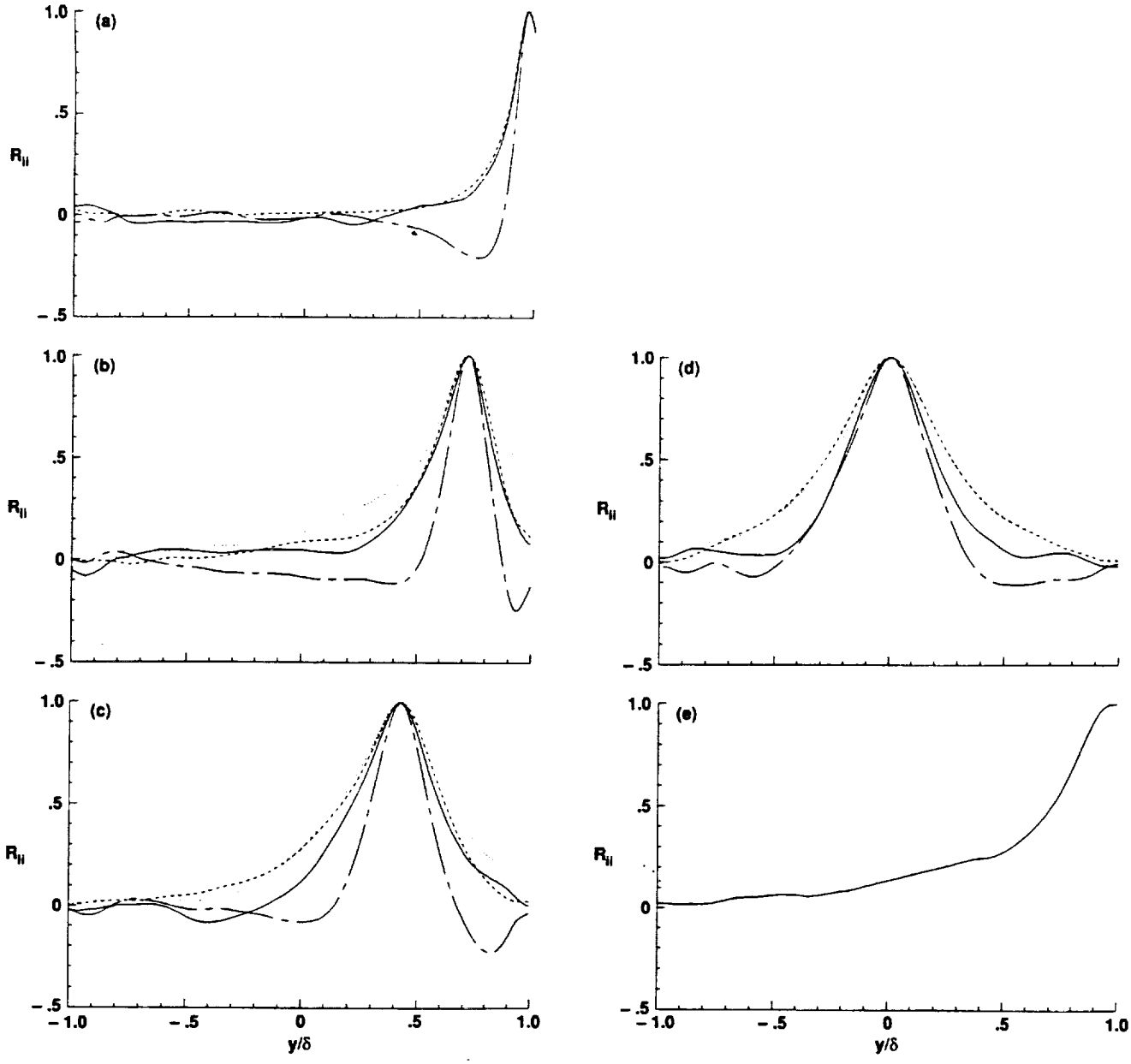

Figure 6. Transverse correlations of perturbations (a) at $y_r^+ \simeq 5$, (b) at $y_r^+ \simeq 50$ (c) at $y_r^+ \simeq 100$, (d) at $y_r^+ \simeq 180$: ——— , R_{uu}; - - - - , R_{vv}; — — — , R_{ww}; ····· , R_{pp}. (e) Transverse correlation of pressure perturbation at $y_r^+ = 0$

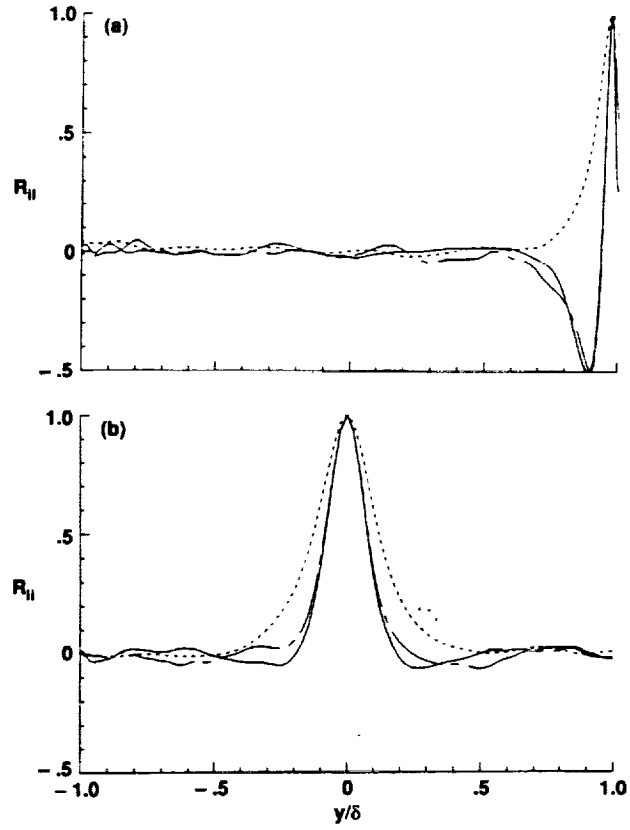

Figure 7. Transverse correlations of perturbations (a) at $y_r^+ \simeq 5$, (b) at $y_r^+ \simeq 180$: ——— , $R_{\omega_x\omega_x}$; - - - - , $R_{\omega_y\omega_y}$; — — — , $R_{\omega_z\omega_z}$.

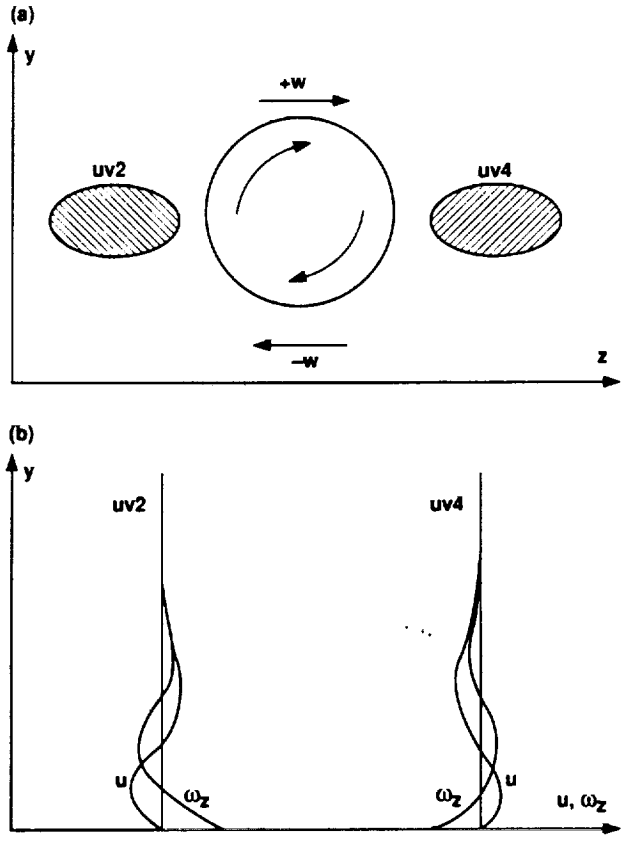

Figure 8. A streamwise vortex and its induced motions.

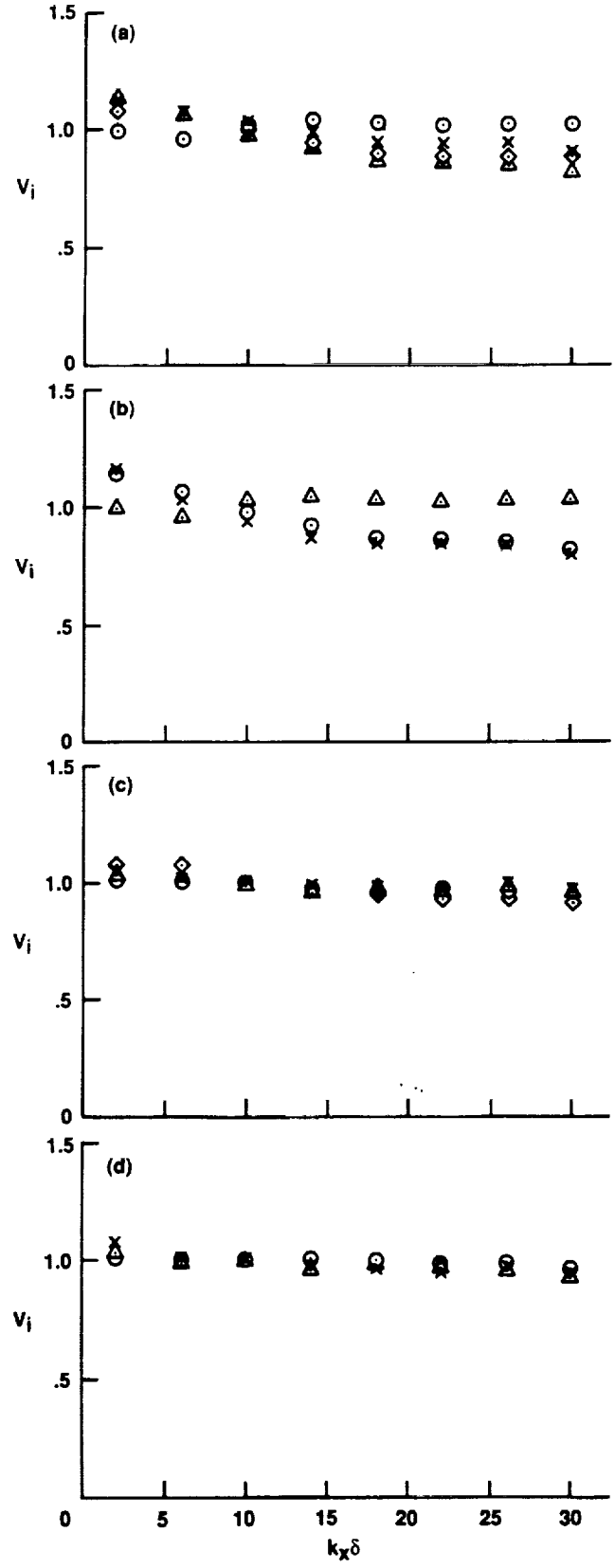

Figure 9. Propagation velocities as a function of the streamwise wavenumbers, k_x. (a) At $y_r^+ \simeq 0.05$: ○ , V_u; △ , V_v; × , V_w; ◇ , V_p. (b) At $y_r^+ \simeq 0.05$: ○ , $V_{\omega_x\omega_x}$; △ , $V_{\omega_y\omega_y}$; × , $V_{\omega_z\omega_z}$. (c) At $y_r^+ \simeq 12$: ○ , V_u; △ , V_v; × , V_w; ◇ , V_p. (d) At $y_r^+ \simeq 12$: ○ , $V_{\omega_x\omega_x}$; △ , $V_{\omega_y\omega_y}$; × , $V_{\omega_z\omega_z}$.

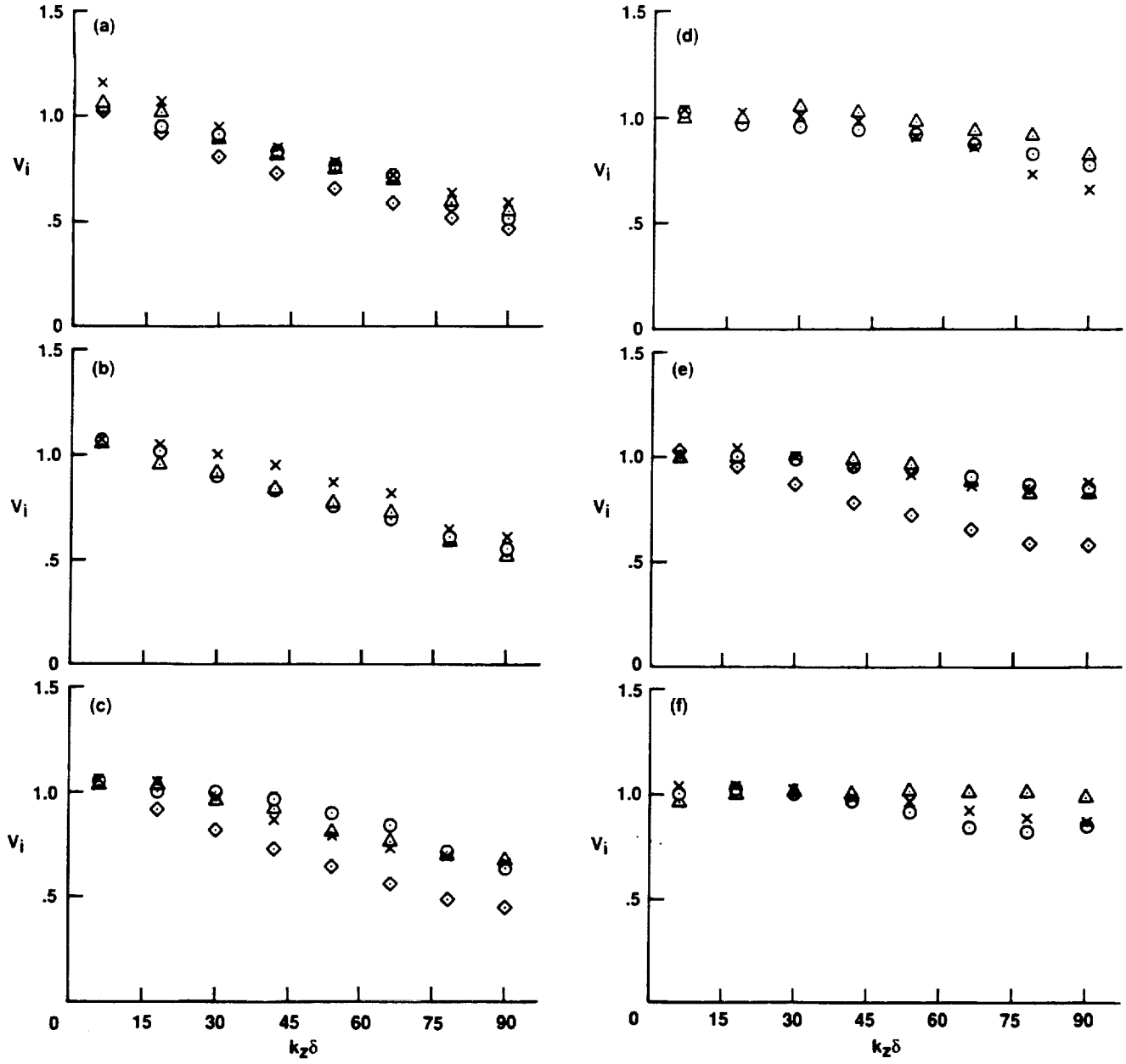

Figure 10. Propagation velocities as a function of the spanwise wavenumbers, k_z. (a) At $y_\tau^+ \simeq 0.05$: o , V_u; $\triangle$, V_v; $\times$, V_w; $\diamond$, V_p. (b) At $y_\tau^+ \simeq 0.05$: o , $V_{\omega_x\omega_z}$; $\triangle$, $V_{\omega_y\omega_y}$; $\times$, $V_{\omega_z\omega_z}$. (c) At $y_\tau^+ \simeq 5$: o , V_u; $\triangle$, V_v; $\times$, V_w; $\diamond$, V_p. (d) At $y_\tau^+ \simeq 5$: o , $V_{\omega_x\omega_x}$; $\triangle$, $V_{\omega_y\omega_y}$; $\times$, $V_{\omega_z\omega_z}$. (e) At $y_\tau^+ \simeq 12$: o , V_u; $\triangle$, V_v; $\times$, V_w; $\diamond$, V_p. (f) At $y_\tau^+ \simeq 12$: o , $V_{\omega_x\omega_x}$; $\triangle$, $V_{\omega_y\omega_y}$; $\times$, $V_{\omega_z\omega_z}$.

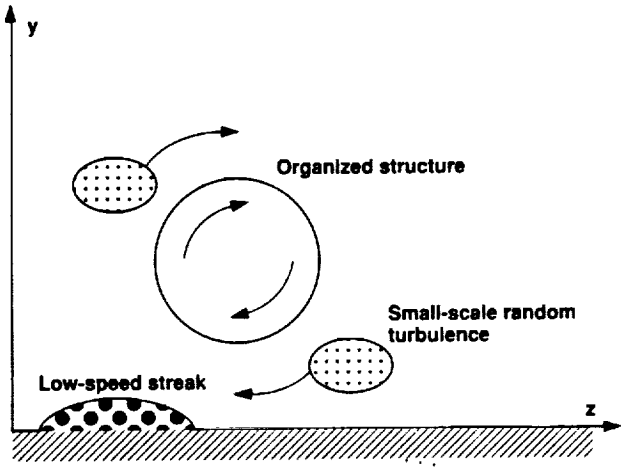

Figure 11. Small-scale (random) turbulence produced near the wall.

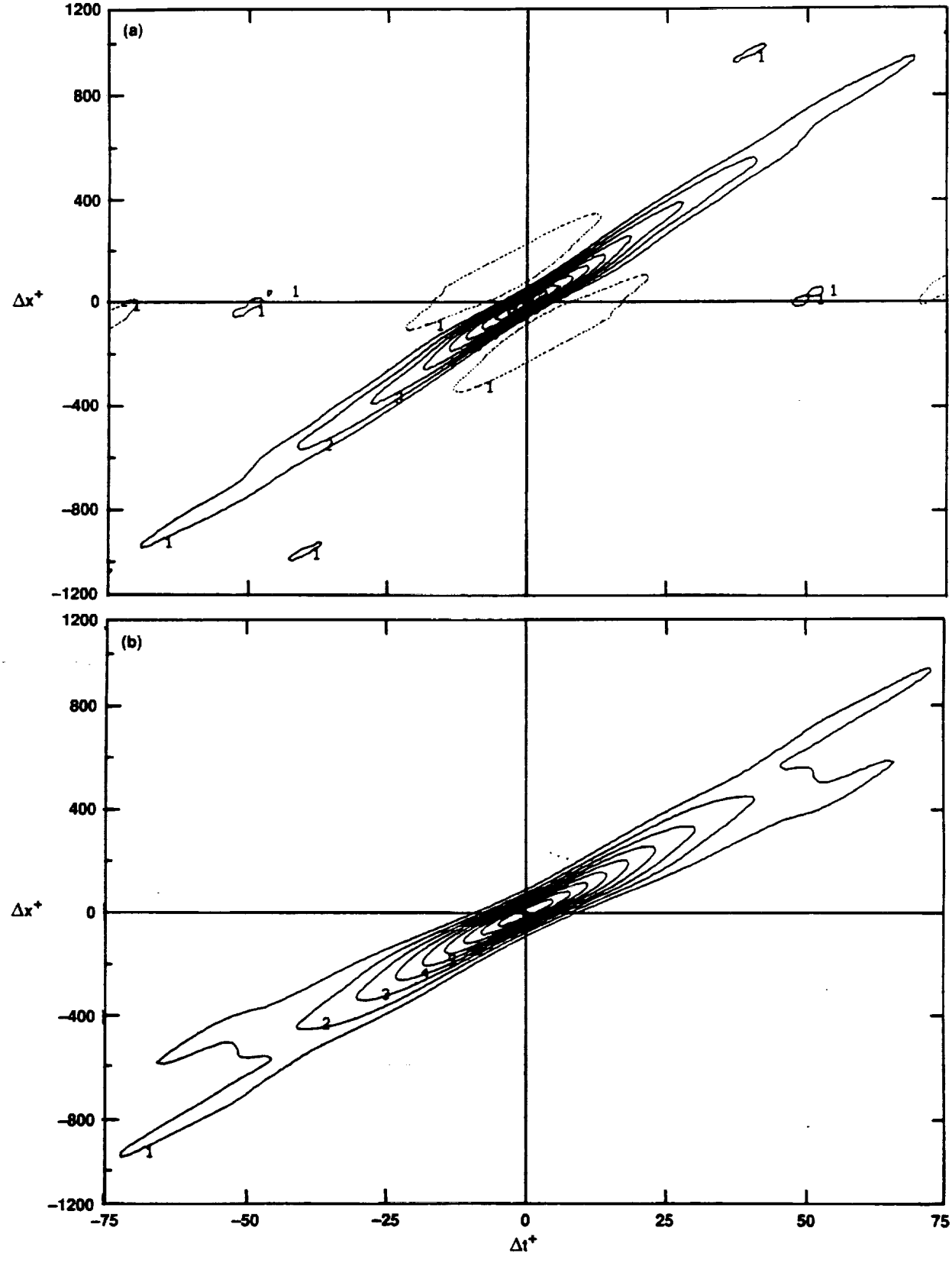

Figure 12. Space-time correlations in the (x, z)-plane at the wall: (a) $R_{pp}(\Delta x, \Delta t)$; (b) $R_{\omega_z\omega_z}(\Delta x, \Delta t)$.

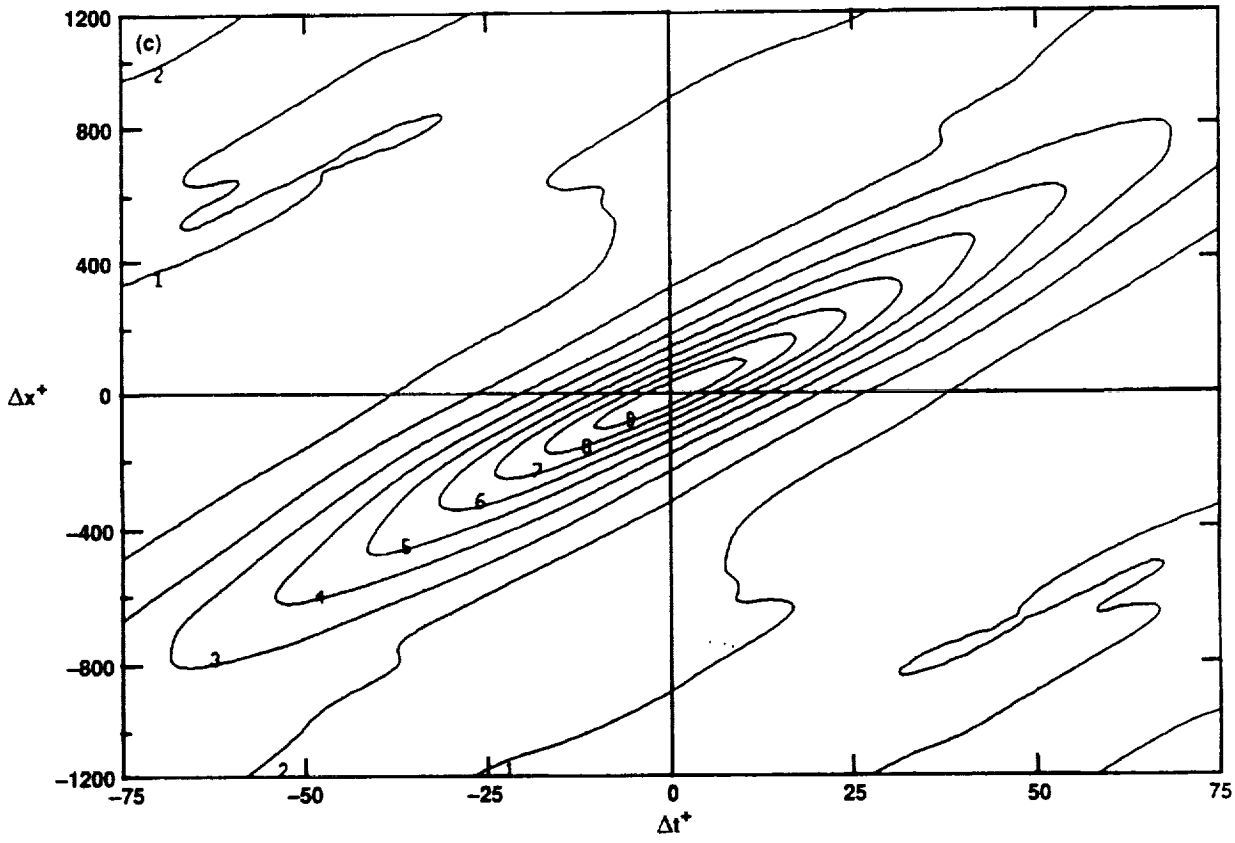

Figure 12. Concluded. (c) $R_{\omega_z\omega_z}(\Delta x, \Delta t)$.

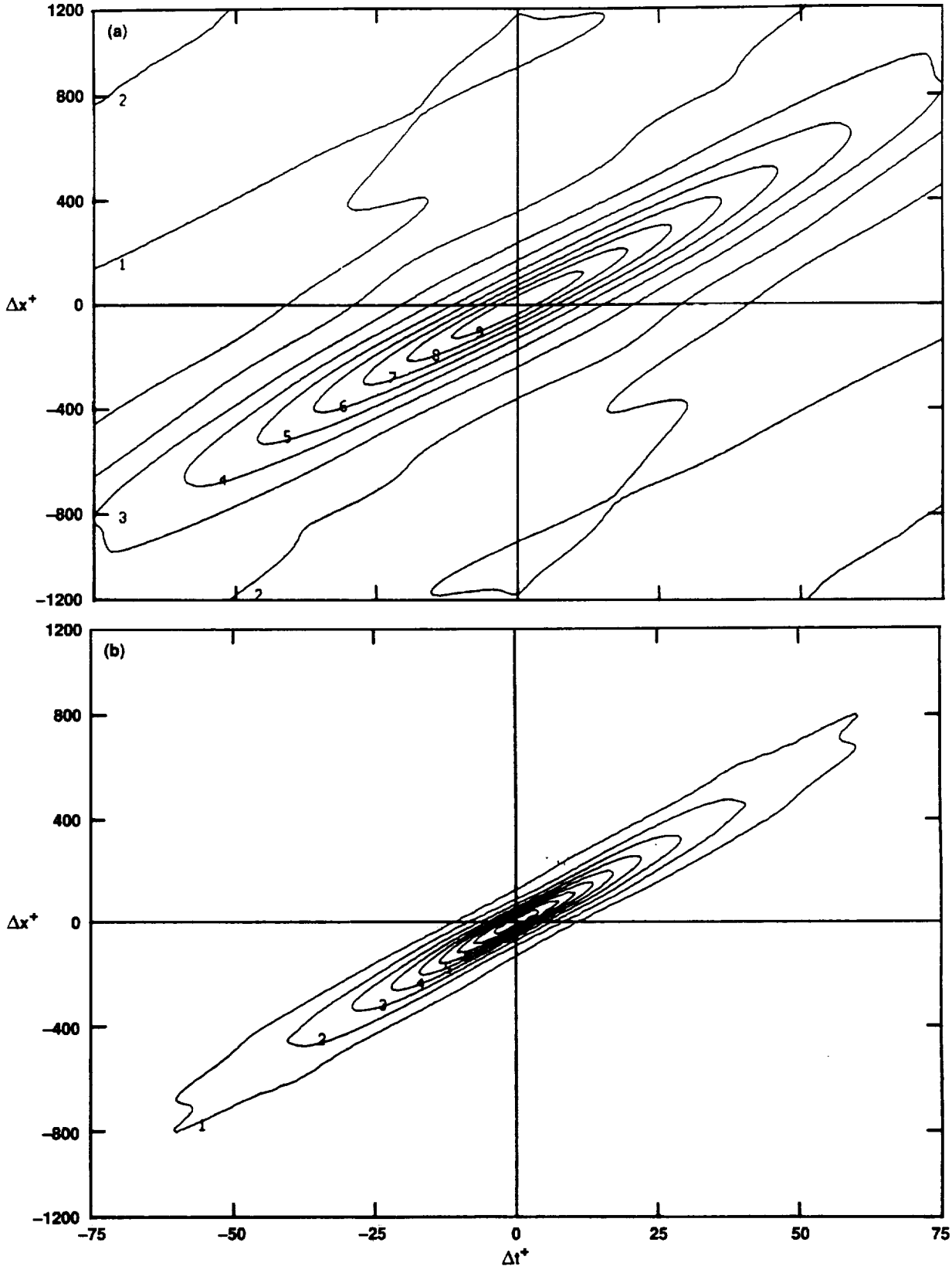

Figure 13. Space-time correlations in the (x, z)-plane at $y^+ \simeq 12$: (a) $R_{uu}(\Delta x, \Delta t)$; (b) $R_{vv}(\Delta x, \Delta t)$.

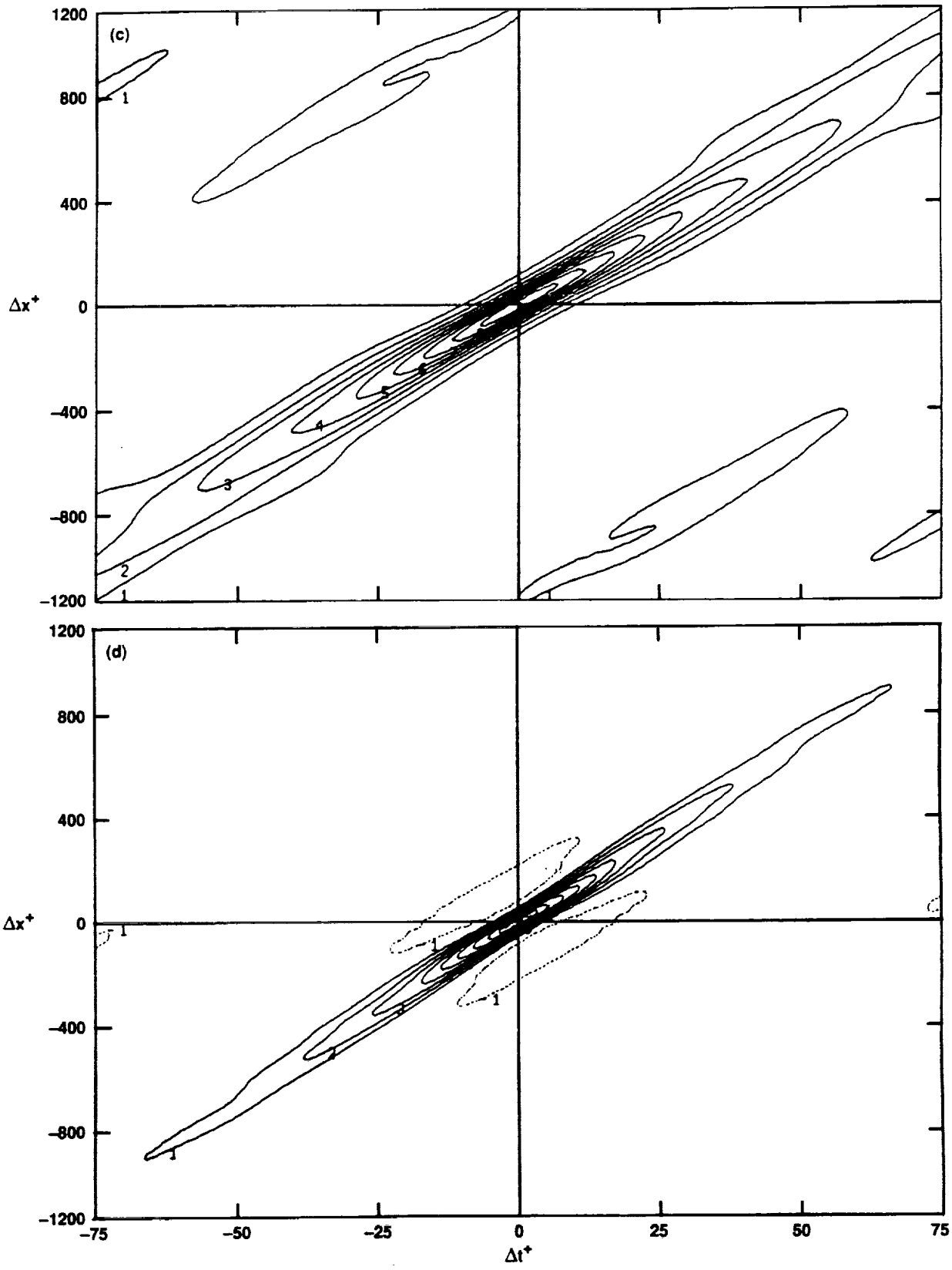

Figure 13. Continued. (c) $R_{ww}(\Delta x, \Delta t)$; (d) $R_{pp}(\Delta x, \Delta t)$.

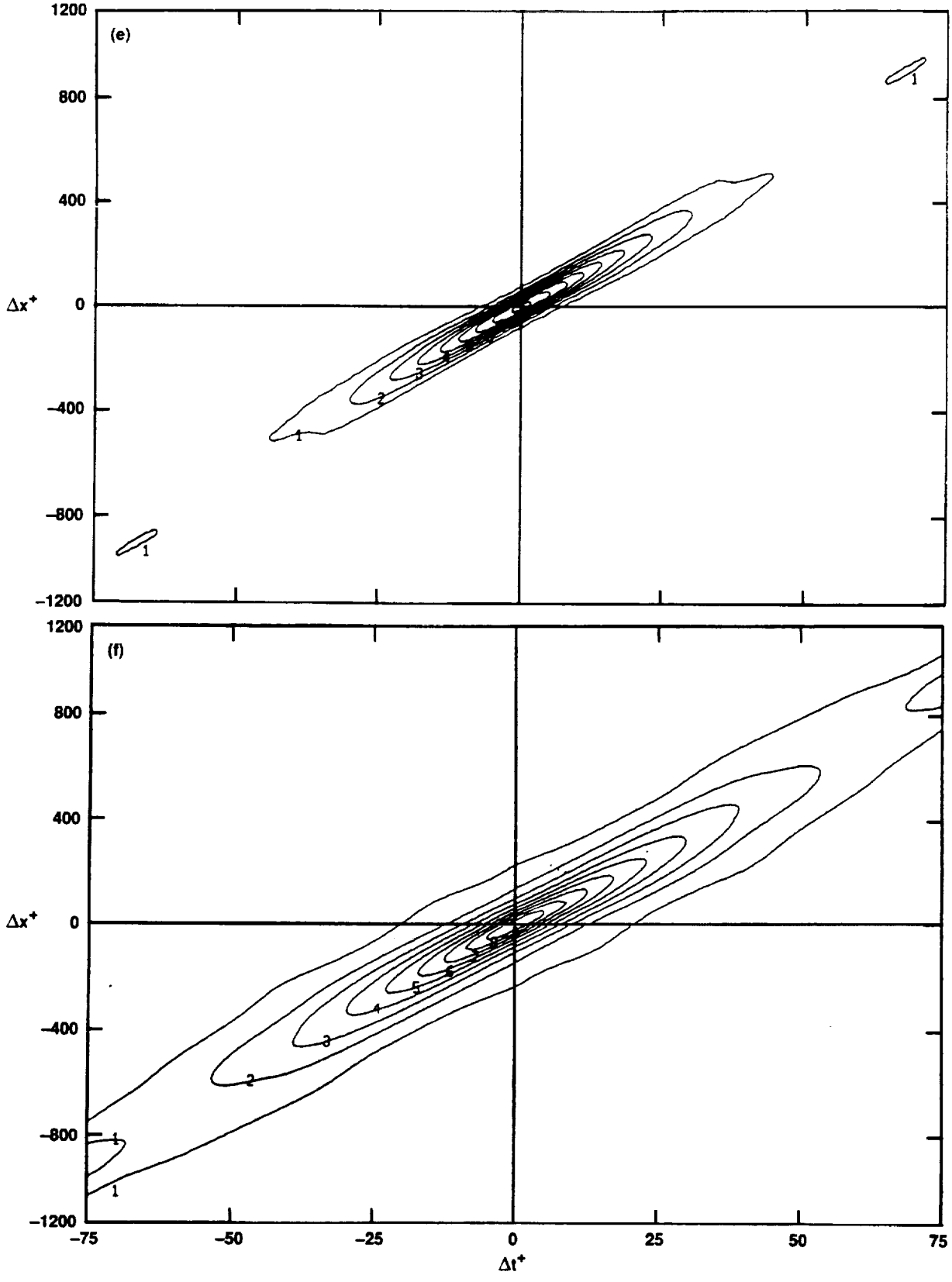

Figure 13. Continued. (e) $R_{\omega_z\omega_z}(\Delta x, \Delta t)$; (f) $R_{\omega_y\omega_y}(\Delta x, \Delta t)$.

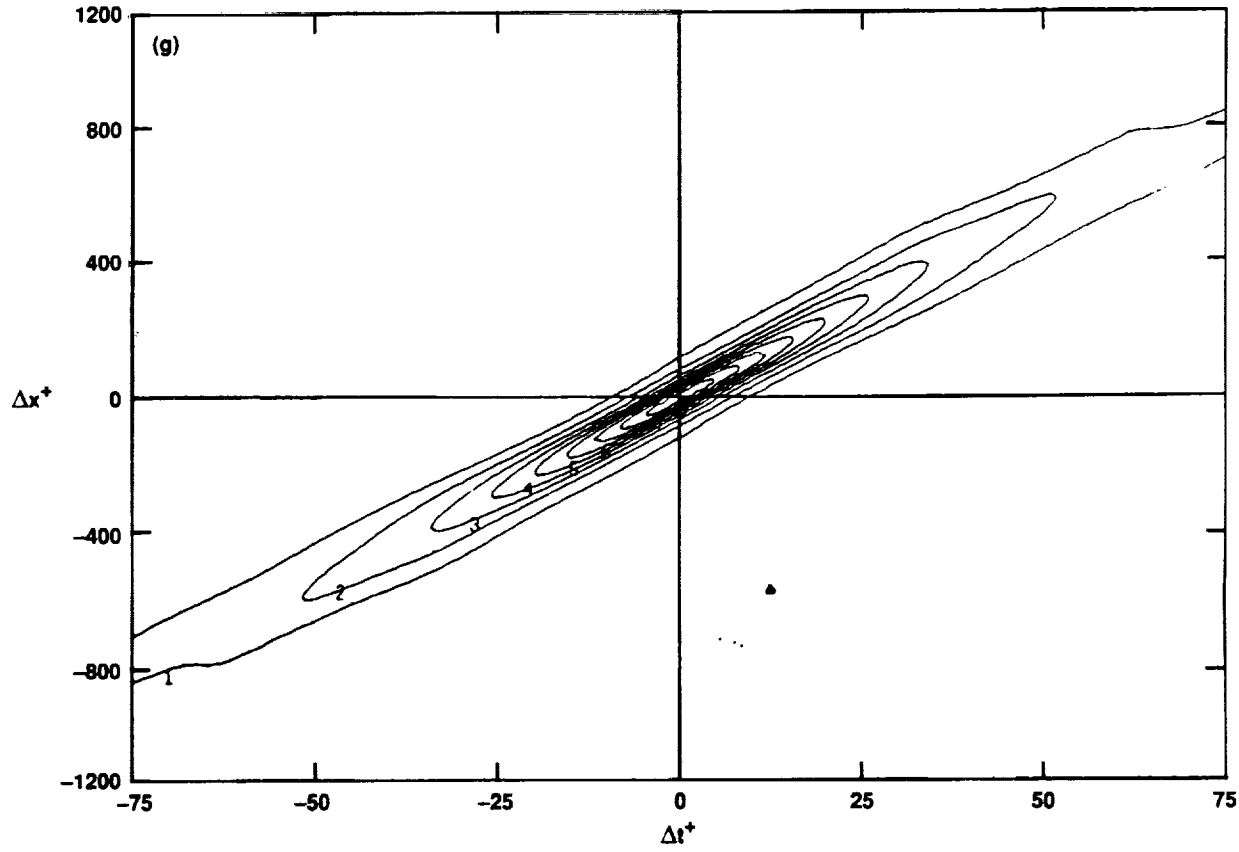

Figure 13. Concluded. (g) $R_{\omega_z\omega_z}(\Delta x, \Delta t)$.

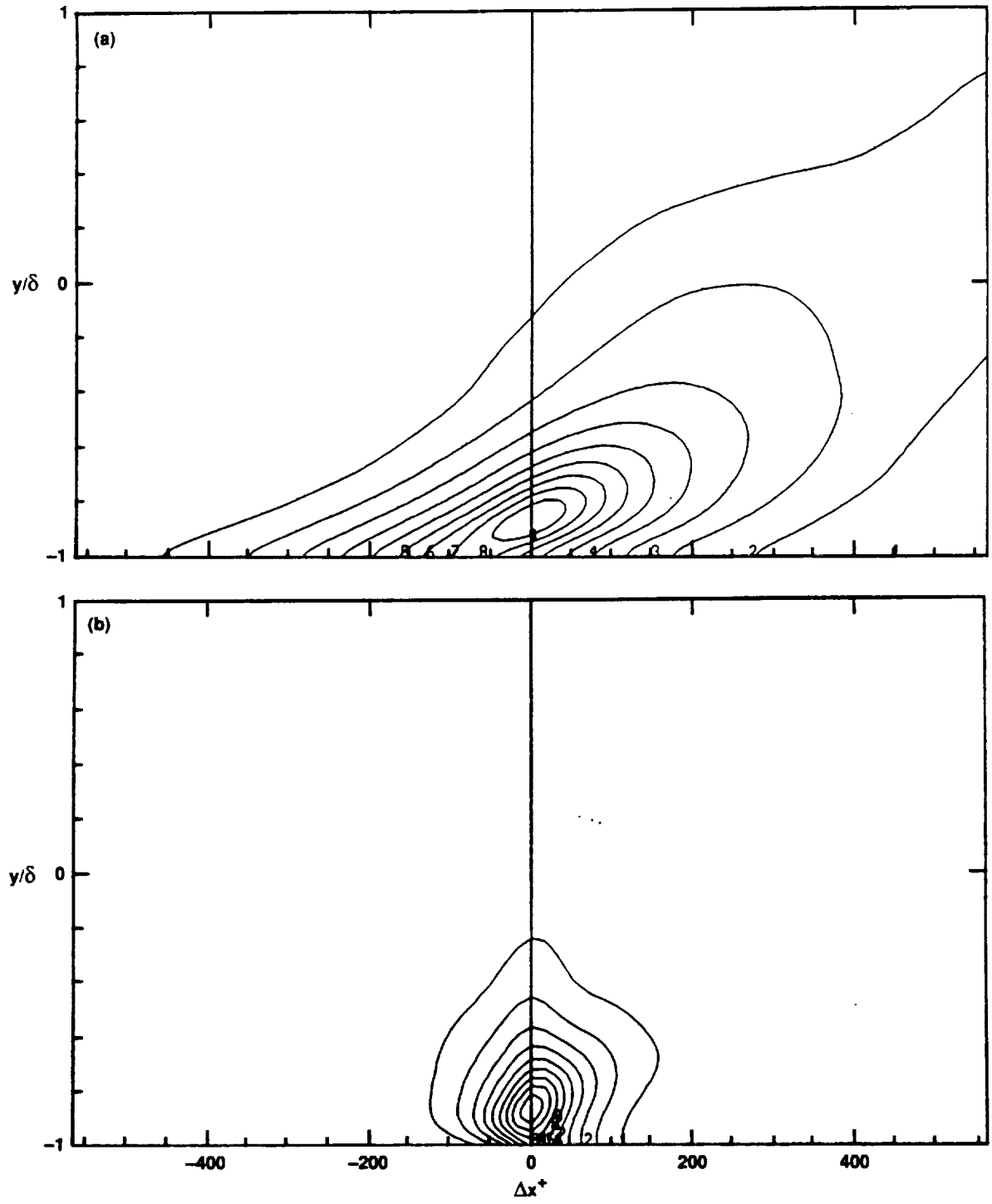

Figure 14. Two-point correlations in the (x, y)-plane for $y_\tau^+ \simeq 12$: (a) $R_{uu}(\Delta x, y)$; (b) $R_{vv}(\Delta x, y)$.

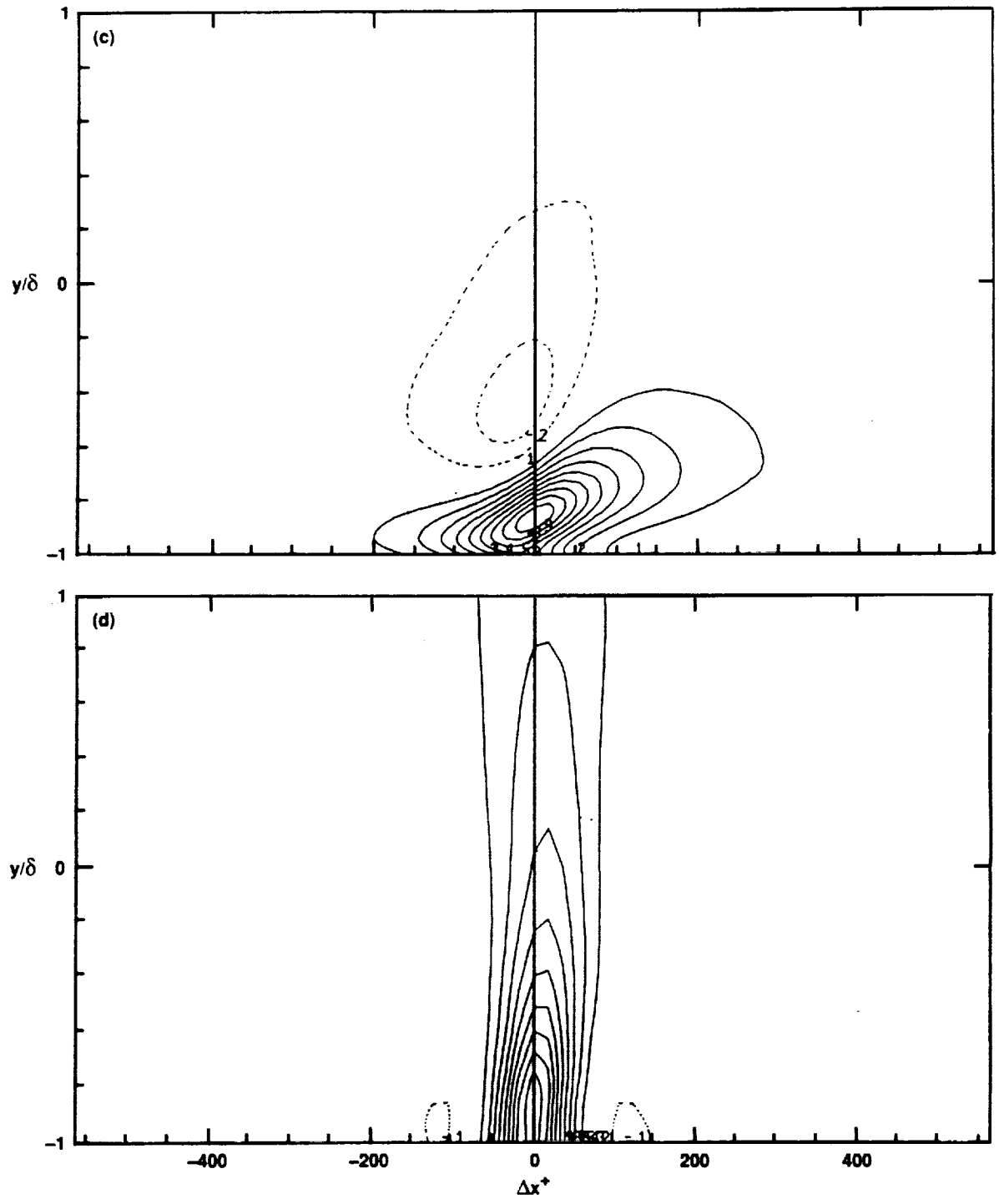

Figure 14. Continued. (c) $R_{ww}(\Delta x, y)$; (d) $R_{pp}(\Delta x, y)$.

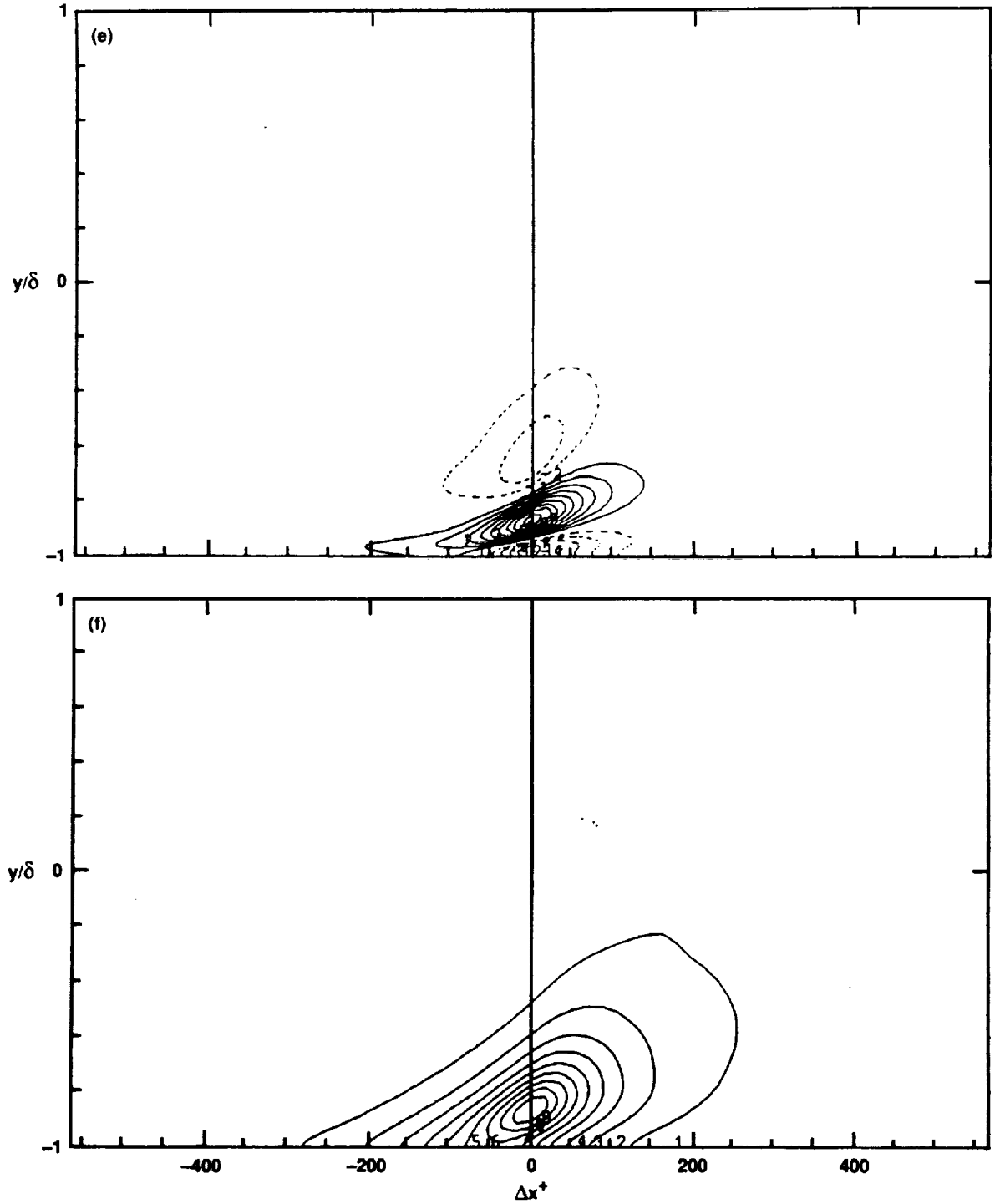

Figure 14. Continued. (e) $R_{\omega_x\omega_x}(\Delta x, y)$; (f) $R_{\omega_y\omega_y}(\Delta x, y)$.

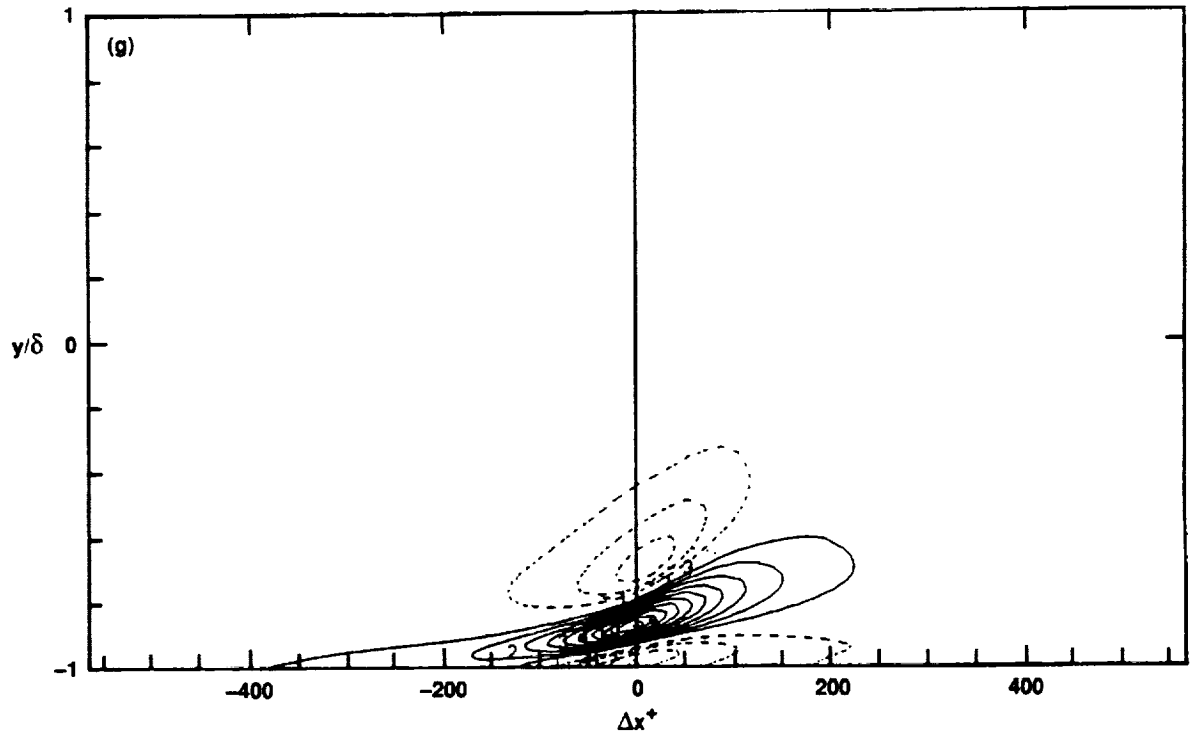

Figure 14. Concluded. (g) $R_{\omega_z\omega_z}(\Delta x, y)$.

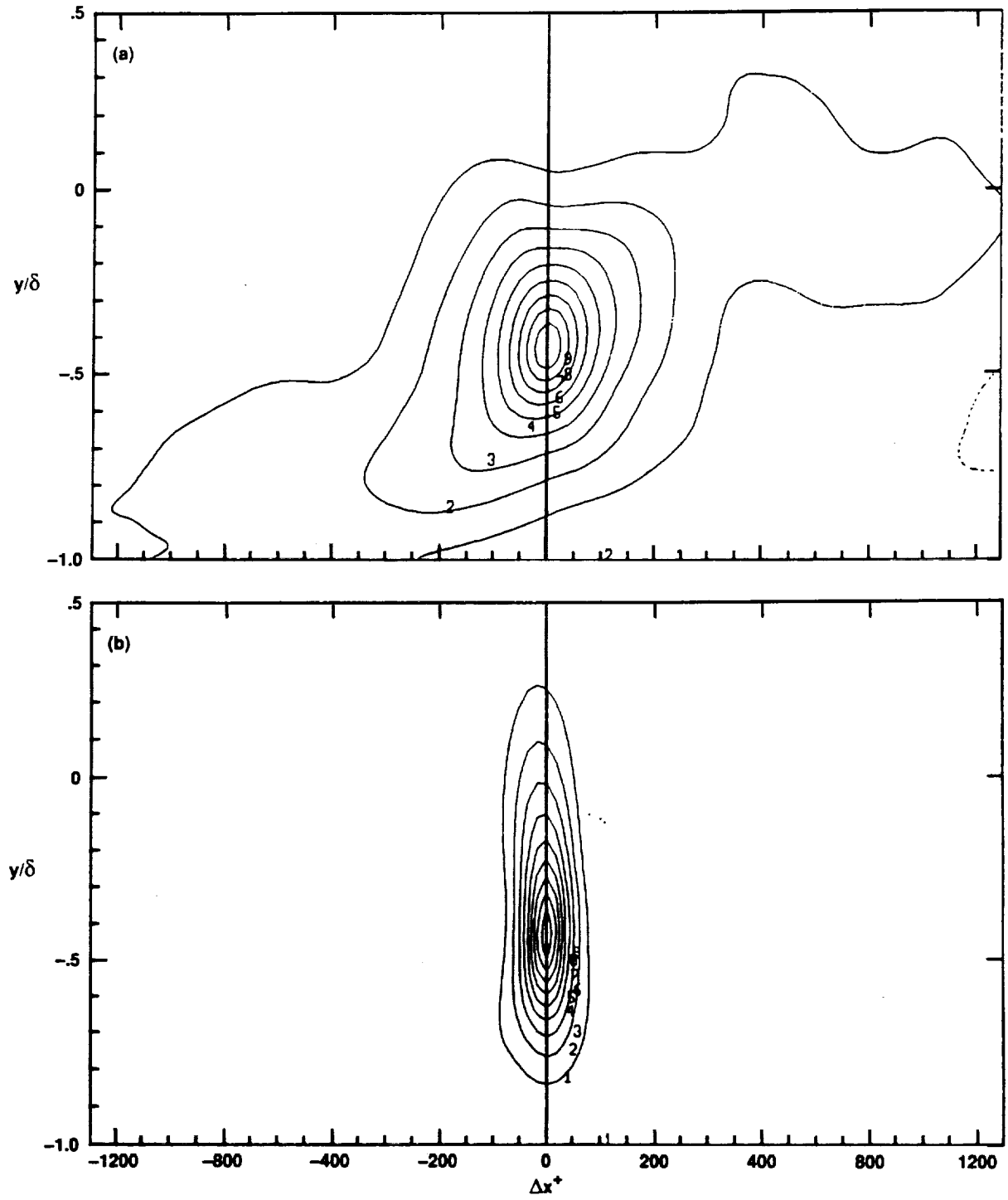

Figure 15. Two-point correlations in the (x, y)-plane for $y_r^+ \simeq 100$: (a) $R_{uu}(\Delta x, y)$; (b) $R_{vv}(\Delta x, y)$.

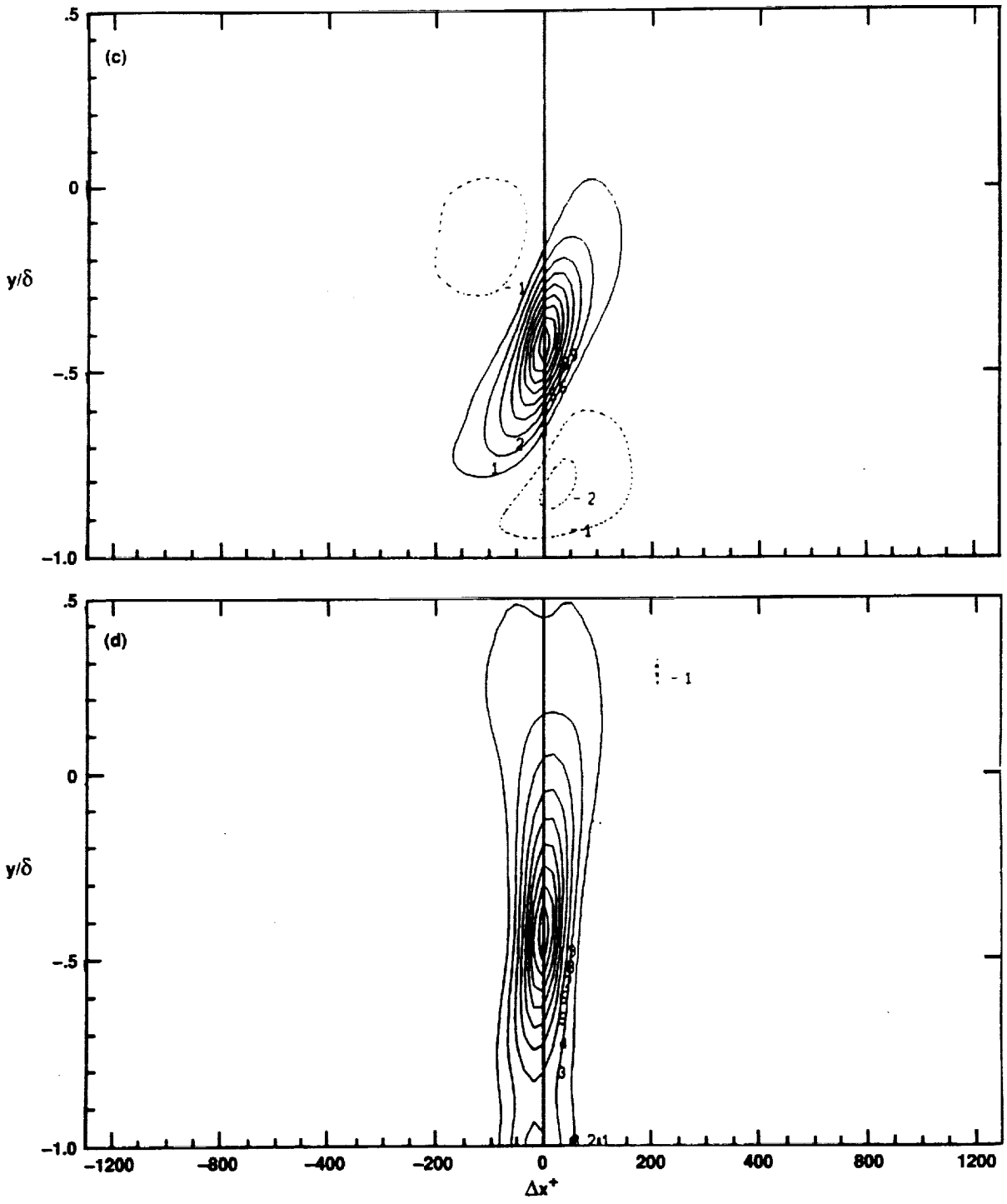

Figure 15. Continued. (c) $R_{ww}(\Delta x, y)$; (d) $R_{pp}(\Delta x, y)$.

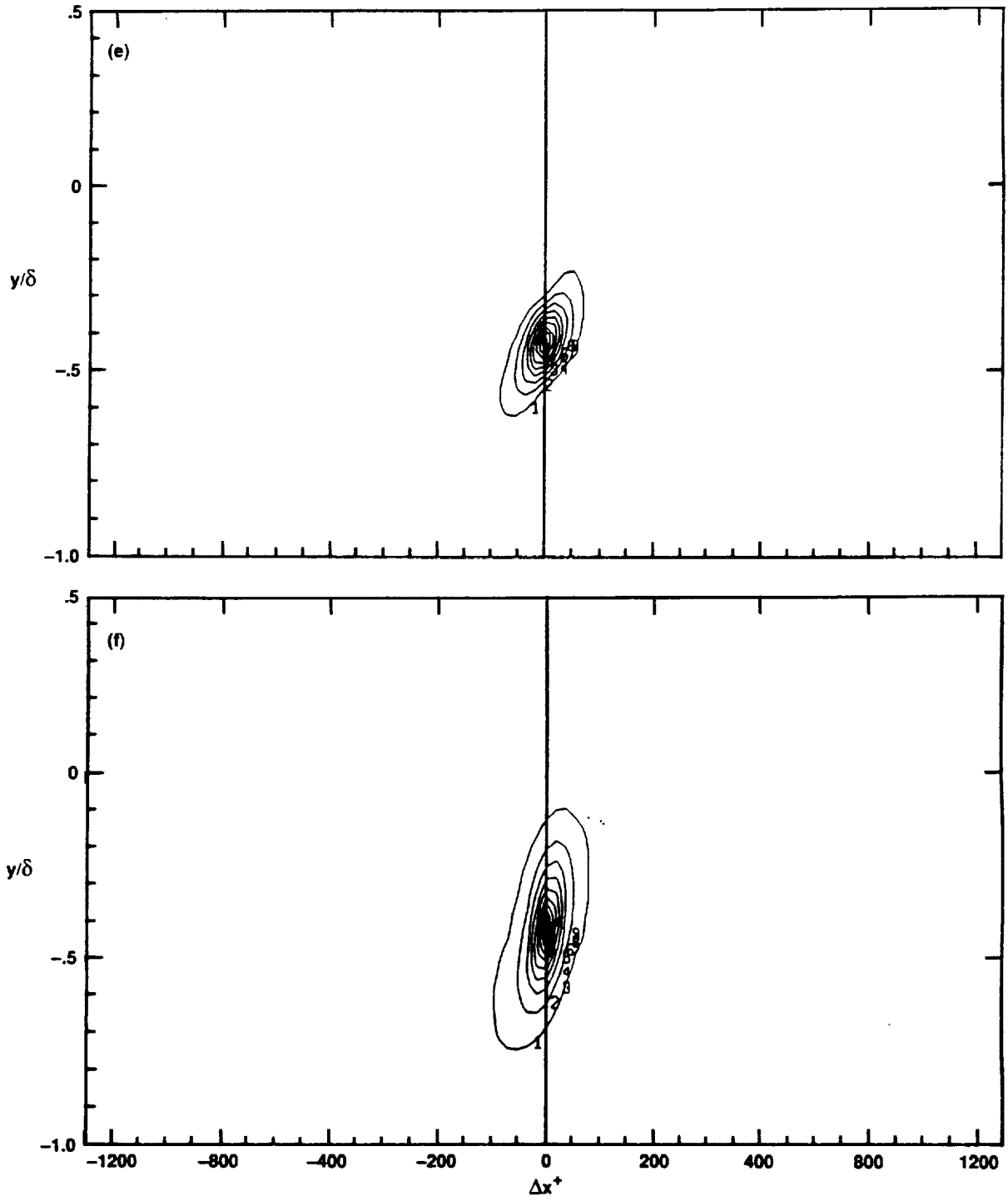

Figure 15. Continued. (e) $R_{\omega_x\omega_x}(\Delta x, y)$; (f) $R_{\omega_y\omega_y}(\Delta x, y)$.

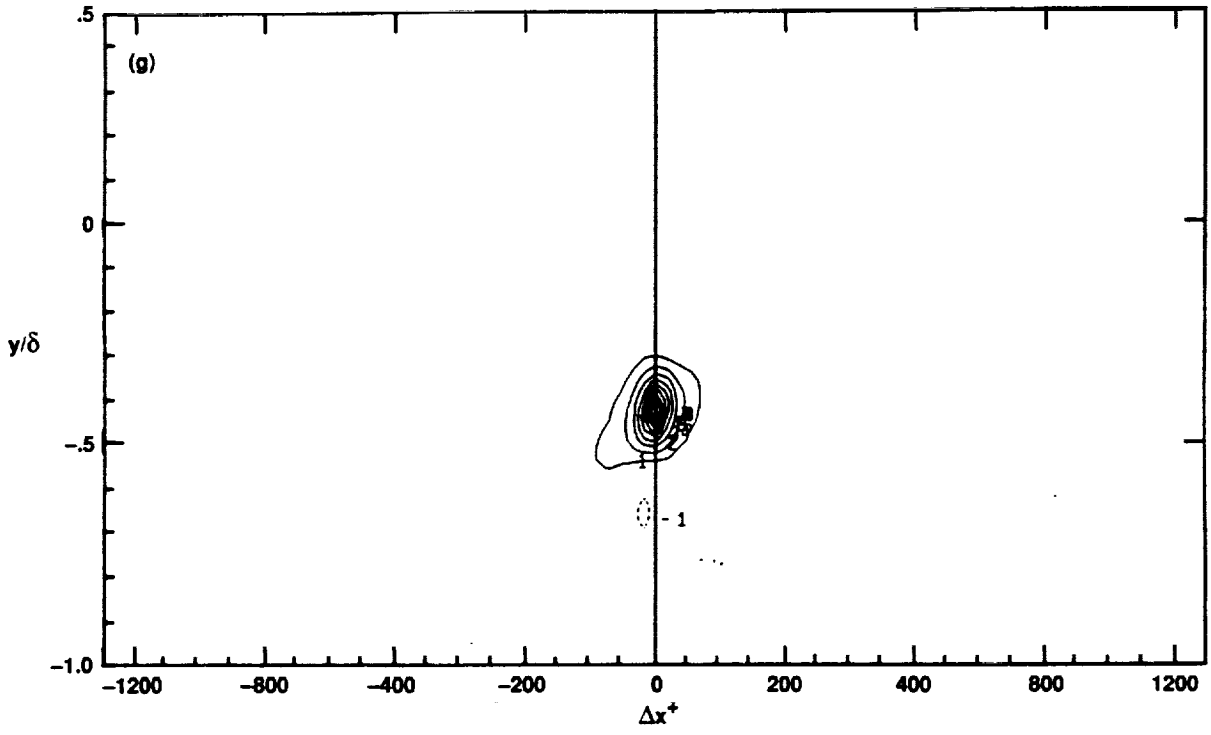

Figure 15. Concluded. (g) $R_{\omega_z\omega_z}(\Delta x, y)$.

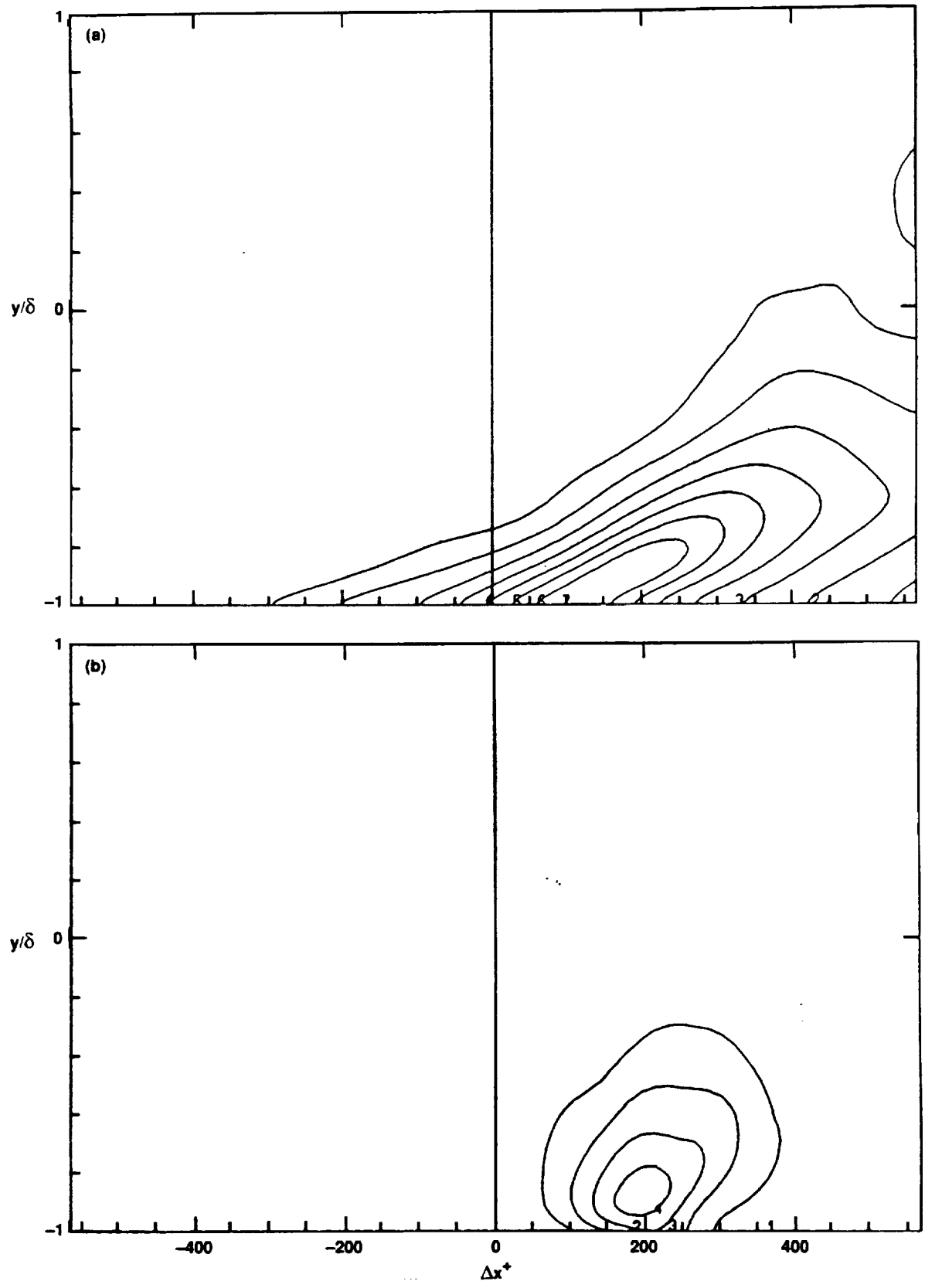

Figure 16. Two-point correlations at nonzero time delay ($\Delta t^+ = 18$) in the (x, y)-plane for $y_r^+ \simeq 12$: (a) $R_{uu}(\Delta x, y)$; (b) $R_{vv}(\Delta x, y)$.

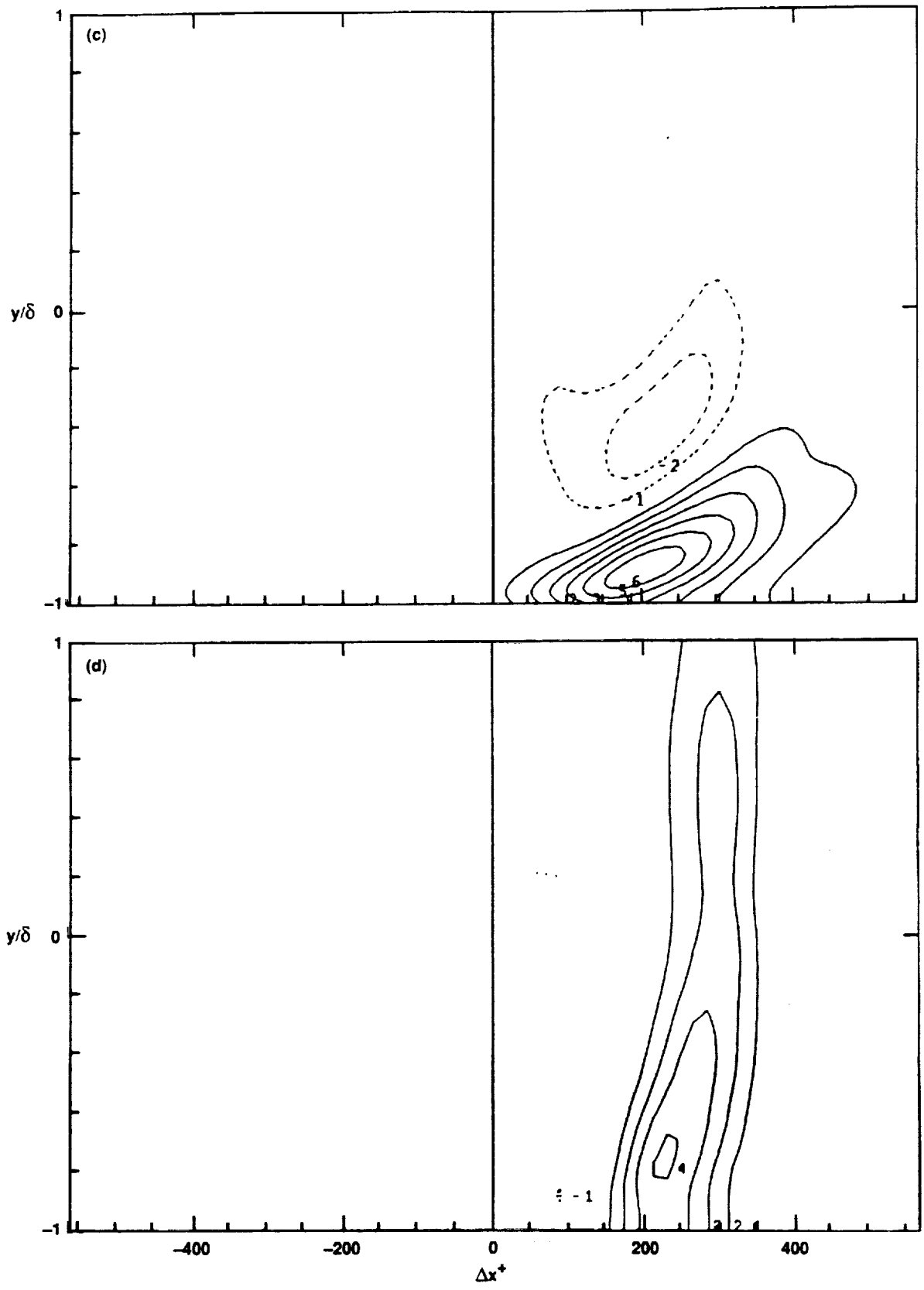

Figure 16. Continued. (c) $R_{ww}(\Delta x, y)$; (d) $R_{pp}(\Delta x, y)$.

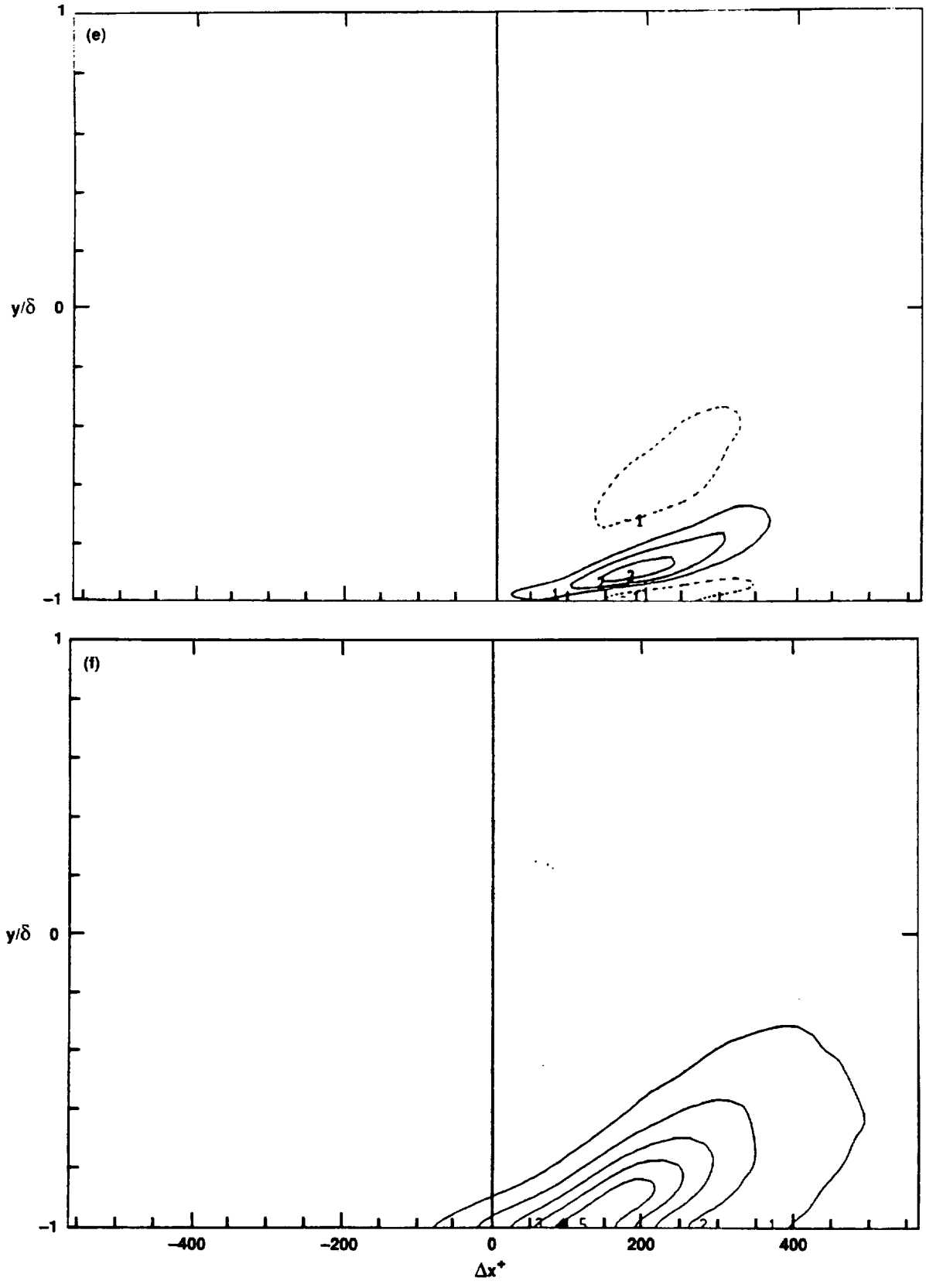

Figure 16. Continued. (e) $R_{\omega_x\omega_x}(\Delta x, y)$; (f) $R_{\omega_y\omega_y}(\Delta x, y)$.

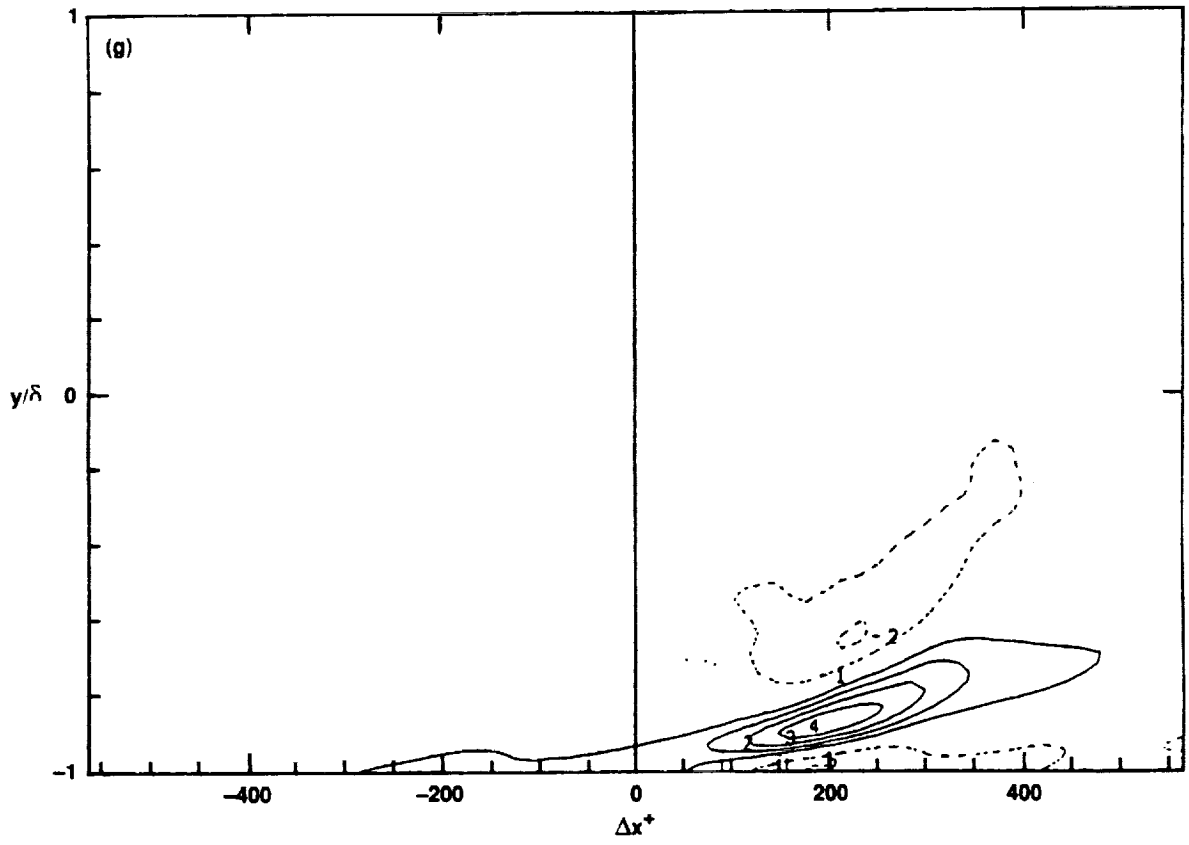

Figure 16. Concluded. (g) $R_{\omega_z\omega_z}(\Delta x, y)$.

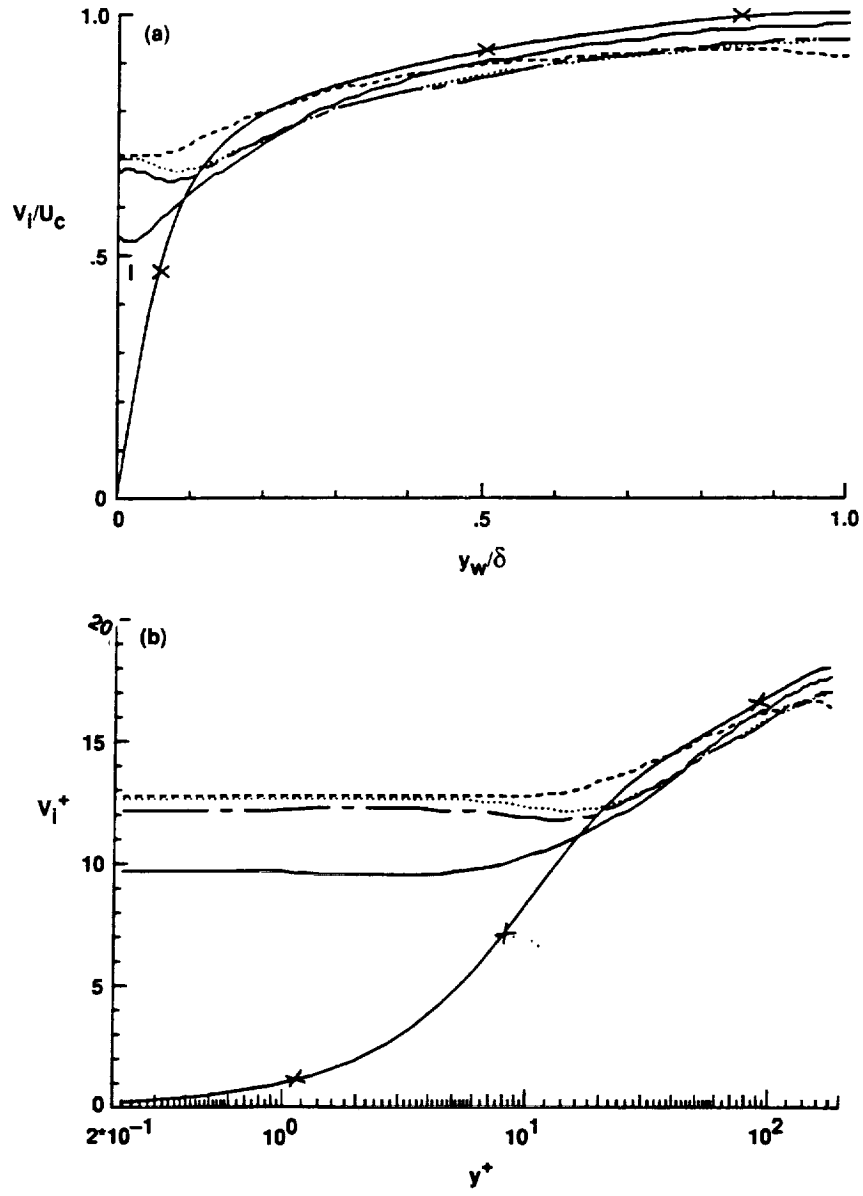

Figure 17. Propagation velocities for the rapid and slow pressure perturbations across the channel (a) in global coordinate and (b) in wall coordinate: —×— , mean; ——— , V_u; - - - - , V_{p_r}; — - — , V_{p_s}; ····· , V_p.

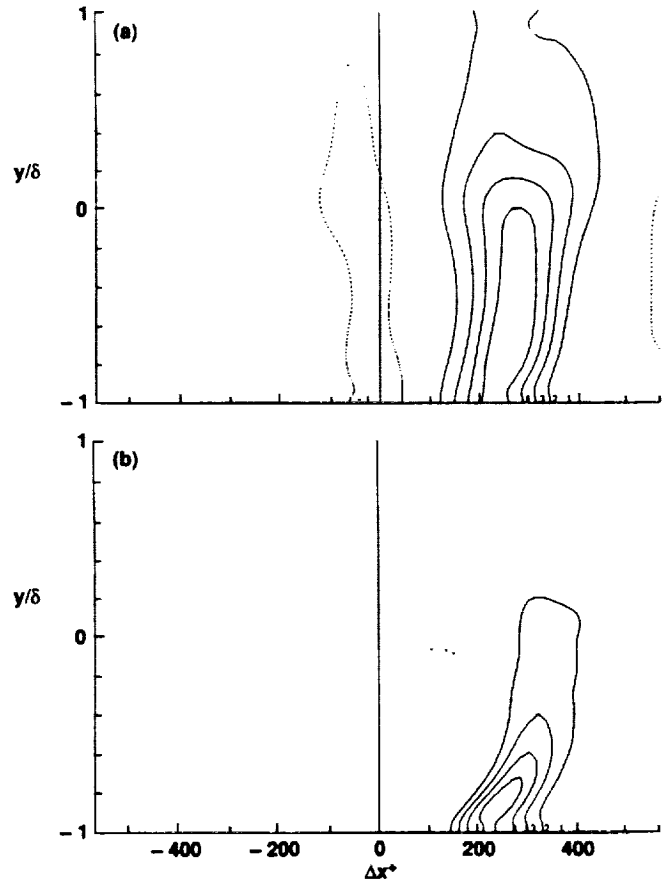

Figure 18. Two-point correlations at nonzero time delay ($\Delta t^+ = 18$) in the (x, y)-plane for $y_r^+ = 0$: (a) $R_{p_r p_r}(\Delta x, y)$; (b) $R_{p_s p_s}(\Delta x, y)$.

REPORT DOCUMENTATION PAGE

Form Approved
OMB No. 0704-0188

1. AGENCY USE ONLY *(Leave blank)*	2. REPORT DATE	3. REPORT TYPE AND DATES COVERED
	May 1992	Technical Memorandum

4. TITLE AND SUBTITLE

Propagation Velocity and Space-Time Correlation of Perturbations in Turbulent Channel Flow

5. FUNDING NUMBERS

505-60

6. AUTHOR(S)

John Kim and Fazle Hussain (University of Houston, Houston, TX 77204)

7. PERFORMING ORGANIZATION NAME(S) AND ADDRESS(ES)

Ames Research Center
Moffett Field, CA 94035-1000

8. PERFORMING ORGANIZATION REPORT NUMBER

A-92088

9. SPONSORING/MONITORING AGENCY NAME(S) AND ADDRESS(ES)

National Aeronautics and Space Administration
Washington, DC 20546-0001

10. SPONSORING/MONITORING AGENCY REPORT NUMBER

NASA TM-103932

11. SUPPLEMENTARY NOTES

Point of Contact: John Kim, Ames Research Center, MS 202A-1, Moffett Field, CA 94035-1000; (415) 604-5867 or FTS 464-5867

12a. DISTRIBUTION/AVAILABILITY STATEMENT

Unclassified — Unlimited
Subject Category 34

12b. DISTRIBUTION CODE

13. ABSTRACT ***(Maximum 200 words)***

A database obtained from direct numerical simulation of a turbulent channel flow is analyzed to extract the propagation velocity V of velocity, vorticity and pressure fluctuations from their space-time correlations. A surprising result is that V is approximately the same as the local mean velocity for most of the channel, except for the near-wall region. For $y^+ \leq 15$, V is virtually constant, implying that perturbations of all flow variables propagate like waves near the wall. In this region V is 55% of the centerline velocity U_c for velocity and vorticity perturbations and 75% of U_c for pressure perturbations. Scale-dependence of V is also examined by analyzing the bandpass-filtered flow fields. This paper contains comprehensive documentation the propagation velocities and space-time correlation data, which should prove useful in the evaluation of Taylor's hypothesis. An attempt has been made to explain some of the data in terms of our current understanding of organized structures, although not all of the data can be explained this way.

14. SUBJECT TERMS

Turbulence, Propagation velocity, Numerical simulation

15. NUMBER OF PAGES

46

16. PRICE CODE

A03

17. SECURITY CLASSIFICATION OF REPORT	18. SECURITY CLASSIFICATION OF THIS PAGE	19. SECURITY CLASSIFICATION OF ABSTRACT	20. LIMITATION OF ABSTRACT
Unclassified	Unclassified		